

## 2. EXPLANATORY NOTES<sup>1</sup>

Shipboard Scientific Party<sup>2</sup>

### INTRODUCTION

In this chapter, we describe the shipboard procedures used during Leg 193. This information concerns only shipboard operations and analyses described in the site chapters of the Leg 193 *Initial Reports* volume of the *Proceedings of the Ocean Drilling Program*. Methods used by various investigators for shore-based analyses of Leg 193 data will be described in the individual scientific contributions to be published in the *Scientific Results* volume and in various professional journals. Abbreviations of technical terms in this volume are listed in Table T1, p. 60.

### Authorship

The Leg 193 Summary chapter and separate sections of the site chapters were written by the following shipboard scientists (authors are listed in alphabetical order; no seniority is implied):

Leg 193 Summary: Fernando Barriga, Ray Binns, Jay Miller  
Operations Summary: Leon Holloway, Gerry Iturrino, Jay Miller, Mike Storms  
Igneous Petrology: Wolfgang Bach, Ray Binns, Jay Miller, Holger Paulick, Dave Vanko, Chris Yeats  
Hydrothermal Alteration: Wolfgang Bach, Fernando Barriga, Ray Binns, Klas Lackschewitz, Dave Vanko, Chris Yeats  
Sulfide and Oxide Petrology: Fernando Barriga, Ray Binns, Terje Bjerkgaard, John Kulange, Álvaro Pinto, Steve Roberts, Steve Scott, Ian Warden, Chris Yeats  
Structural Geology: Terje Bjerkgaard, Bob Findlay  
Geochemistry: Wolfgang Bach, Fernando Barriga, Liane Benning, Ray Binns, Erika Elswick, Jay Miller, Dave Vanko  
Microbiology: Ryuji Asada, Hiro Kimura, Andrew Masta

---

T1. Abbreviations of technical terms, p. 60.

---

<sup>1</sup>Examples of how to reference the whole or part of this volume.

<sup>2</sup>Shipboard Scientific Party addresses.

Physical Properties: Lizet Christiansen, Gerry Iturrino  
Rock Magnetism: Sang-Mook Lee  
Downhole Measurements: Anne Bartetzko, Gerry Iturrino

The summary core descriptions (“barrel sheets”), core photographs, and thin-section descriptions can be accessed from the “[Core Descriptions](#)” contents list.

## Shipboard Scientific Procedures

### Numbering of Sites, Holes, Cores, and Samples

The Ocean Drilling Program (ODP) drill sites are numbered consecutively and each site consists of one or more holes drilled while the ship was positioned over one acoustic beacon. For all ODP drill sites, a letter suffix distinguishes individual holes drilled at the same site. The first hole to be drilled is assigned the site number modified by the suffix A, the second hole takes the site number and suffix B, and so forth. Note that this procedure differs slightly from that used by the Deep Sea Drilling Project (DSDP; Sites 1 through 624), but prevents ambiguity between site- and hole-number designations.

The cored interval is measured in meters below seafloor (mbsf). The depth interval assigned to an individual core begins with the depth below the seafloor at which the coring began and extends to the depth that the coring ended. Each coring interval is generally  $\leq 9.5$  m, which is the length of a core barrel. Coring intervals may be shorter and may not necessarily be adjacent if separated by drilled intervals that are not cored.

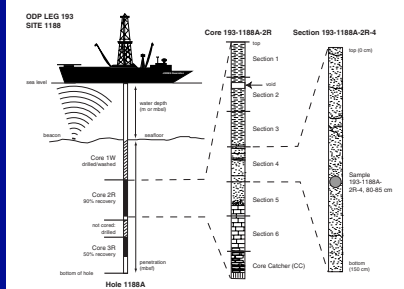
Cores taken from a hole are numbered sequentially from the top of the hole downward. Core numbers and their associated cored intervals (in mbsf) are unique in a given hole. Normally, maximum recovery for a single core is 9.5 m of rock or sediment contained in a plastic liner (6.6-cm internal diameter) plus  $\sim 0.2$  m (without a plastic liner) in the core catcher (Fig. F1). The core catcher is a device at the bottom of the core barrel that prevents the core from sliding out when the barrel is being retrieved from the hole.

A recovered core is divided into 1.5-m sections that are numbered serially from the top (Fig. F1). When full recovery is obtained, the sections are numbered from 1 through 7, with the last section possibly being shorter than 1.5 m. When less than full recovery is obtained, as many sections as are needed to accommodate the length of the core are used (e.g., 4 m of core would be divided into two 1.5-m sections and a 1-m section). If cores are fragmented and recovery is  $<100\%$ , sections are numbered serially and the rest of the drilled interval is regarded as void, whether or not shipboard scientists think that the fragments were contiguous when in situ. In rare cases, a section  $<1.5$  m in length may be cut to preserve features of interest visible through the core liner (e.g., lithologic contacts).

By convention, material recovered from the core catcher is placed below the last section. The core catcher is placed at the top of the cored interval in cases where material is recovered only in the core catcher. However, information supplied by the drillers or by logging may allow for a more precise interpretation as to the correct position of core-catcher material within an incompletely recovered cored interval.

Also by convention, when the recovered core is shorter than the cored interval, the top of the core is equated with the top of the cored

F1. Schematic examples of numbered core sections, p. 39.



interval. Samples taken from the cores are designated by distance measured in centimeters from the top of the section to the top and bottom of each sample.

A complete identification number for a sample consists of the following information: leg, site, hole, core number, core type, section number, piece number (for hard rock), and interval in centimeters measured from the top of the section. For example, a sample identification of “Sample 193-1188A-1R-4, 80–85 cm” indicates a 5-cm sample removed from the interval between 80 and 85 cm below the top of Section 4, Core 1 (R designates that this core was taken during rotary drilling) of Hole 1188A during Leg 193 (Fig. F1).

## **Core Handling**

### **Igneous and Hydrothermally Altered Rocks**

There were special handling and curation requirements for all cores recovered during Leg 193. Plastic core liners were split into nominally 1.5-m lengths and total core recovery calculated by shunting the rock pieces together and measuring the total length in each section to the nearest centimeter. This information was logged into the shipboard Corelog database program as liner length (length of the plastic liner) and curated length (length of core inside the liner). The plastic core liner containing each section was sealed at the top and bottom by gluing on color-coded plastic caps: blue to identify the top of a section and translucent to identify the bottom. Caps were attached to the liner by coating the end of the liner and the inside rim of the cap with acetone. The core was then transferred into the core laboratory.

Because microbiological sampling was a primary objective of Leg 193, special precautions were taken to minimize contamination of the cores prior to sampling. Anyone handling the core prior to microbiological sampling wore latex gloves swabbed in alcohol. The contents of each section were transferred into 1.5-m-long sections of split core liner, and with the oversight of a co-chief scientist or designate, an interval of core was identified where appropriate for microbiological sampling. Because this interval had not been described, it was photographed on the core table with a handheld digital camera, and if deemed necessary a brief description was prepared. The whole-round section or piece was then transferred to the microbiology laboratory for processing. A representative length of Styrofoam was used to mark the location of the sampled interval in the split core liner. Residues from the microbiological sampling were returned to the core liner after processing, and we attempted to accurately curate these using the digital images and descriptions as guides.

After microbiological sampling, the bottom of oriented pieces (i.e., pieces that clearly could not have rotated top to bottom about a horizontal axis in the liner) were marked with a red wax pencil. This was to ensure that orientation was not lost during splitting and labeling. Contiguous pieces of the core with obvious features that allowed alignment were curated as a single piece and plastic spacers were affixed between pieces and/or reconstructed pieces in the core liner. In some cases, when we were concerned that structural features might be lost during core splitting, cores were photographed as whole rounds (see the “[Core Descriptions](#)” contents list). The core was passed through the shipboard multisensor track (MST) and then split into archive and working halves, either with a diamond saw or as described below for disinte-

grated core. For sawed core, each piece was numbered sequentially from the top of each section, beginning with number 1; reconstructed pieces were all assigned the same number, but with a consecutive suffix letter (e.g., Piece 1A, 1B, etc.). Pieces were labeled only on the outer cylindrical surfaces of the core. If the piece was oriented, that is, the piece was long enough that it could not have rotated about its long axis in the core liner, an arrow was added to the label pointing to the top of the section.

Many initially continuous core samples taken with the advanced diamond core barrel (ADCB) during Leg 193 tended to disintegrate during or after removal from the core barrel (see Fig. F2A, F2B). For curation, equivalent collections of fragments were placed into the working and archive halves, and “piece boundaries” were set at detectable changes in lithology. Because of this, digital photographs of the cores were taken immediately after recovery. Summary “prelogs” were also prepared to allow effective curation of the cores. These logs and images are presented in the “[Core Descriptions](#)” contents list.

In splitting the core, every effort was made to ensure that important features were represented in both halves. The archive half was described visually, then photographed with both black-and-white and color film, one core at a time. Nondestructive physical properties measurements, such as magnetic susceptibility, were performed on the archive half of the core. The working half was sampled for shipboard physical properties measurements, paleomagnetic studies, inductively coupled plasma-atomic emission spectroscopy (ICP-AES), X-ray diffraction (XRD), and thin-section studies. The working half of the hard-rock core was subsequently sampled for shore-based laboratory studies. Records of all samples are kept by the curator at ODP. Both halves of the core were shrink-wrapped in plastic to prevent rock pieces from vibrating out of sequence during transit, placed into labeled plastic tubes, sealed, and transferred to cold-storage space aboard the drilling vessel. Cores containing sulfides were placed in foil bags, evacuated, and filled with a nitrogen atmosphere prior to final packaging to minimize oxidation. All Leg 193 cores are housed at the Gulf Coast Repository of the Ocean Drilling Program at Texas A&M University.

## **IGNEOUS PETROLOGY**

### **Core Curation and Shipboard Sampling**

To preserve important compositional and structural features in both the archive and working halves, we generally examined the whole core sections containing igneous rocks prior to cutting them with a diamond-impregnated saw. Nondestructive physical properties measurements, such as magnetic susceptibility and natural gamma-ray emission, were made on the core before it was split (see “[Physical Properties](#),” p. 21). After the core was split and described, the working half was sampled for shipboard physical properties measurements, magnetic studies (see “[Rock Magnetism](#),” p. 25), thin sections, XRD, and ICP-AES analyses. The archive half was described on the visual core description (VCD) form and photographed. To minimize contamination of the core with platinum-group elements and gold, scientists and technicians removed jewelry from hands and wrists prior to handling.

To provide a preliminary estimate of the composition of igneous rock units, a refractive index (RI) measurement was made where fresh glass

F2. Fragmented ADCB core, p. 40.



was encountered in core. Small chips were gently crushed and an appropriate size fraction (20–50 μm) obtained by rolling across paper. Aliquots were immersed successively in standard Cargille RI oils (0.002 spacings) and examined under transmitted light with a petrological microscope until the RI was matched or bracketed using the color-dispersed Becke line method in unfiltered white light. Because we expected to be dealing with a consanguineous lava sequence where most major elements are correlated with silica, RI and SiO<sub>2</sub> content were linearly related. A calibration curve (Fig. F3) based on analyzed rocks from the Eastern Manus Basin dredge hauls (R.A. Binns, unpubl. data) was then used to estimate composition. From prior experience, as much as 20% of microlites can be present in the vitreous groundmass without seriously affecting this relationship insofar as it is used to classify the rock type. The following weight percent SiO<sub>2</sub>/RI boundaries (volatile-free basis) were adopted, following the International Union of Geological Sciences (IUGS) scheme (Le Maitre, 1976):

- Basalt - Basaltic andesite boundary at 52 wt% SiO<sub>2</sub>, RI = 1.582;
- Basaltic andesite - Andesite boundary at 58 wt% SiO<sub>2</sub>, RI = 1.558;
- Andesite - Dacite boundary at 63 wt% SiO<sub>2</sub>, RI = 1.538; and
- Dacite - Rhyodacite boundary at 70 wt% SiO<sub>2</sub>, RI = 1.508.

The term rhyodacite is preferred over rhyolite because of the Na/K values and the general lack of quartz phenocrysts.

Where appropriate, mineral phenocryst compositions were similarly estimated using RI calibration charts of Deer et al. (1992, fig. 159). Preliminary petrological observations using crushed particles mounted in oil were also used in several instances where quick information was required for description purposes or where thin-section manufacture was impractical or not intended.

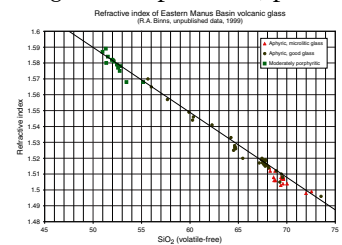
All of the igneous rocks cored during Leg 193 were felsic lavas. Felsic lavas are composed of both coherent and volcanoclastic facies, corresponding to the insulated central part of the erupted melt and the outer brecciated part of the flow, respectively. The relative proportions of coherent and clastic facies of individual flows are variable depending on factors such as temperature, volatile content, viscosity, shear stress, and eruption rate. In subaerial settings, brecciation of the outer part of the lava is a result of autoclastic fragmentation caused by the movement of the ductile center of the flow. In contrast, quench fragmentation is generally considered to be the dominant process in the submarine environment generating hyaloclastite (Figs. F4, F5).

However, surficial lava structures on the crest of Pual Ridge indicate a fluid style of eruption with little evidence of quench fragmentation (Waters et al., 1996).

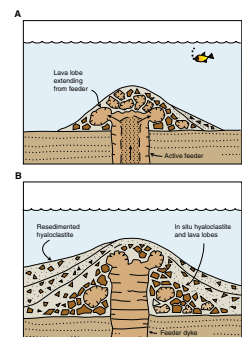
Lavas may show a porphyritic texture with phenocrysts set in a fine-grained or glassy groundmass, or otherwise they may be aphyric, as are most dacites previously sampled from the crest of Pual Ridge. Because phenocrysts are formed in the magma chamber prior to eruption, they are a good indicator of geochemical composition and may be used for correlation and discrimination of individual flows.

The groundmass of felsic lavas can be glassy, vesicular to pumiceous, spherulitic, microcrystalline, or a mixture of several texturally distinctive domains (Fig. F6). In particular, the coherent facies, representing the slowly cooled central part of a flow, may show considerable textural variation. At slow cooling rates, high-temperature devitrification can

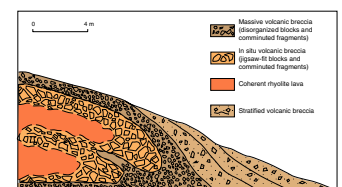
F3. Calibration curve used to estimate glass compositions, p. 42.



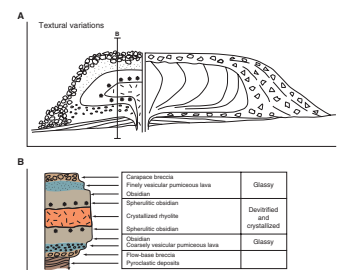
F4. In situ and resedimented hyaloclastite and feeder dike, p. 43.



F5. Schematic volcanic facies associated with subaqueous emplacement of siliceous lava, p. 44.



F6. Schematic cross section through a subaerial silicic lava flow, p. 45.



take place, resulting in the formation of spherulites (round, nodular, or lenticular aggregates of fine quartz and feldspar needles). At even slower cooling rates, an interlocking mosaic of quartz and feldspar crystals would form in the groundmass, but no such samples were encountered in Leg 193 cores. After solidification, glassy parts of the lava are readily altered by interaction with circulating solutions. Perlitic cracks are the result of hydration and volume expansion of the glass representing an early stage of alteration. Typical alteration minerals in diagenetically altered felsic volcanic glass are zeolites, clays minerals, and/or secondary feldspar, depending on temperature and burial depth.

### Visual Core Descriptions

We used VCD forms to document each section of the igneous rock cores. The left column on the form, adjacent to the core photograph, represents the archive half graphically. A horizontal line across the entire width of the column denotes a plastic spacer (see “**Core Handling,**” p. 3). Oriented pieces are indicated on the form by an upward-pointing arrow to the right of the piece. Locations of samples selected for shipboard studies are indicated in the column headed “Shipboard studies” with the following notation: XRD = X-ray diffraction analysis; ICP-AES = inductively coupled plasma-atomic emission spectrometry analysis; TSB = polished petrographic thin section billet; PP = physical properties measurements; and PMAG = paleomagnetic measurements. Lithologic, alteration, and mineralization features are indicated with graphics on the form in three labeled columns (Fig. F7).

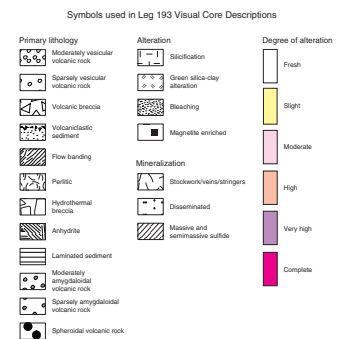
We subdivided the core into consecutively numbered lithologic units on the basis of changes in color, structure, brecciation, grain size, vesicle abundance, mineral occurrence, and abundance. Where possible, unit boundaries were chosen to reflect primary igneous or volcanologic characteristics. However, where processes of alteration obliterated the primary features, units were delineated according to alteration characteristics.

Written descriptions accompany the schematic representation of the core sections. They include the following:

1. The leg, site, hole, core, type, and section number (e.g., 193-1188A-15R-3).
2. The unit number (consecutive downhole), the rock name (see below), and the piece numbers. We assigned provisional rock names on the basis of hand-specimen observation (hand lens and binocular microscope) and RI determinations, and these names were later checked with studies of thin sections. Porphyritic rocks were named by phenocryst type, and descriptors were defined as follows:
  - Aphyric: phenocrysts constitute <1 vol% of the rock,
  - Sparsely phytic: phenocryst content ranges between 1 and <2 vol%, and
  - Moderately phytic: phenocryst content ranges between 2 and <10 vol%.

These descriptors were further modified by including the names of phenocryst phases, in order of decreasing abundance. Thus, a moderately plagioclase-pyroxene-phyric dacite contains between 2 and 10 vol% phenocrysts with the dominant phenocryst being plagioclase with lesser amounts of pyroxene. The

**F7.** Key to the lithologic patterns in the visual core descriptions, p. 46.



- minerals named include all of the phenocryst phases that are present in the rock, as long as the total content is >1%.
3. Contact relations and unit boundaries. The recognition of unit boundaries and description of contact relations are of crucial importance for the interpretation of the emplacement mode of individual units. We were prepared to recognize and describe numerous types of both sharp and gradational contacts, such as those illustrated in Figures F4, F5, and F6. However, no distinctive contacts were cored. In the absence of recovered contacts, different units were chosen based on abrupt changes in rock structure or texture between separate core pieces. In particular, recognition of substantial differences in the phenocryst assemblage (type, abundance, and size range) on either side of a missing contact was used as important evidence for the interpretation of individual lava units.
  4. Phenocrysts. The types of minerals visible with a hand lens or binocular microscope and their distribution within the unit, and for each phase its abundance (by volume percent), size range (in millimeters), shape, degree of alteration, and further comments if appropriate.
  5. Groundmass texture and grain size: glassy, perlitic, spherulitic, aphanitic, fine grained (<1 mm), medium grained (1–5 mm), or coarse grained (>5 mm). Grain size changes within units were also noted.
  6. Vesicles.
    - a. Vesicle abundance (i.e., nonvesicular [no visible vesicles], sparsely vesicular [<5%], and moderately vesicular [5%–20%]). Visual estimates of the volume fraction of vesicles were supplemented by observations using a binocular microscope. Filled vesicles, or amygdules, were noted as well, using the analogous terms sparsely amygdaloidal and moderately amygdaloidal.
    - b. Size and size distribution, including multiple modes if present.
    - c. Shape (sphericity and angularity).
  7. Color (for the dry rock surface).
  8. Rock structure. This is determined by whether the unit is massive, has a chilled margin(s), is flow banded, brecciated, or volcanoclastic. The term “volcanoclastic rock” encompasses any clastic unit composed predominately of volcanogenic particles. Before the core first arrived on deck, we reviewed the following information and prepared an appropriate description strategy. In general, volcanic fragments are generated during explosive volcanic activity (e.g., plinian, strombolian, or phreatomagmatic eruptions) producing pyroclasts or by autobrecciation (autoclasts) and quench fragmentation (hyaloclastite) during emplacement of a lava flow. Commonly, primary volcanoclastic deposits (e.g., fall deposits, pyroclastic flow deposits, in situ autobreccia) consist of loose material that is readily eroded, and hence, volcanic fragments may become part of the rock units emplaced by sedimentary processes. Every effort was made to ensure we distinguished different types of primary volcanoclastic deposits, resedimented volcanoclastic units emplaced by sedimentary processes, and hydrothermally generated breccias.

However, in cases where the evidence is ambiguous, strictly descriptive nomenclature was applied exclusively (see below).

- Descriptive nomenclature. The names for individual rock units are based on the lithologic observations using a strictly descriptive scheme proposed by McPhie et al. (1993). Ideally, these names provide a short, nongenetic description of the rock that includes features like composition, grain size, texture, lithofacies, and alteration (e.g., fresh, poorly sorted, monomictic vitric breccia). In addition, genetic nomenclature (e.g., in situ hyaloclastite) is used where appropriate. For coherent lavas the names are based on an estimate of the composition, lithofacies observations, texture, and alteration (Fig. F8). Volcaniclastic rocks are classified according to grain-size measurements (or estimates), components of the rock, lithofacies observation, and alteration (Fig. F9).

### Thin-Section Descriptions

We examined thin sections from the core intervals noted on the VCD forms to complement and refine the hand-specimen observations. In general, the same terminology was used for thin-section descriptions as for the VCDs. The percentages of individual phases were estimated visually, and reported in the thin-section descriptions (see the “Core Descriptions” contents list). The textural terms used are defined by MacKenzie et al. (1982). Thin sections of volcaniclastic rocks that were sufficiently fresh to allow the discrimination of vesicles, phenocrysts, and groundmass were point counted using an automatic point counter and a regular rectangular grid.

For some porphyritic rocks, the thin-section analyses and VCDs differ slightly, typically because small plagioclase laths in a rock with seriate texture are visible only in thin section. Thus, for example, a rock described visually as olivine-plagioclase-phyric may be plagioclase-olivine-phyric in the thin-section description. Similarly, vitric and lithic components may be estimated incorrectly in volcaniclastic hand samples, and therefore a different rock name assigned to a thin section as a result. Thin sections were described for as many units as was practical, although it was not possible to produce sections for every unit defined.

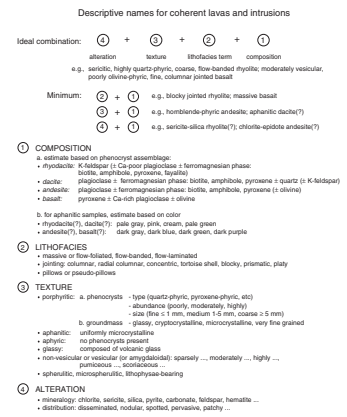
### HYDROTHERMAL ALTERATION

Almost all the rocks recovered during Leg 193 have undergone hydrothermal alteration. On the hard-rock VCD forms and the alteration and mineralization logs, rocks were graded according to whether they are fresh (<2% by volume alteration products) or have slight (2%–<10%), moderate (10%–<40%), high (40%–<80%), very high (80%–<95%), or complete (95%–100%) alteration. Alteration and vein/structure core description logs on a piece-by-piece scale were tabulated to provide a consistent characterization of the rocks and to quantify vein abundance and alteration intensity.

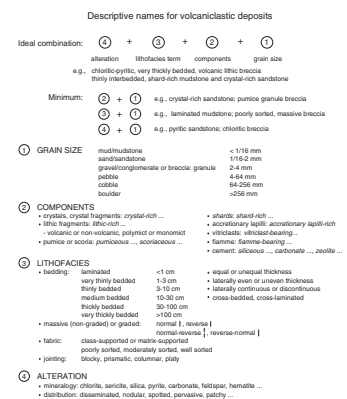
### Description of Altered Material

Alteration/mineralization and vein/structure descriptions for each hole are found in the “Core Descriptions” contents list. These were based mostly on visual and binocular microscope observations of cut,

F8. Scheme for assigning descriptive names for coherent lavas and intrusions, p. 47.



F9. Scheme for assigning descriptive names for volcaniclastic deposits, p. 48.



wet surfaces, and specific alteration minerals were only distinguished where it was considered that unequivocal identification could be made. Where additional mineralogical evidence was available from RI and/or XRD measurements (see below), these identifications were integrated into the alteration/mineralization spreadsheets and the VCD forms. However, we did not enter these data into the vein/structure spreadsheet. Table T2 provides a list of abbreviations used in alteration/mineralization and vein/structure descriptions.

We recorded the following information in the alteration/mineralization and vein/structure description sheets:

1. The alteration/mineralization spreadsheet (e.g., Table T3) was used to record the bulk-rock alteration. Each entry records the lithostratigraphic unit and identifiers for the core, section, piece, interval, the length of each piece, and the curated depth below seafloor of the top of each piece. Visual estimates of the rock color (dominant and secondary), alteration intensity (as recorded on the VCD), alteration style (pervasive, patchy, stockwork, vein-style, or vesicle fill), alteration type (as determined by hand-specimen and thin-section observations), and grain size were recorded for each segment. Columns were available to record the abundance of the principal nonsulfide alteration minerals, plus any others, where identifiable. A separate section of the form was provided to summarize the style, grain size, and abundance of any sulfide minerals present in the core interval. More detailed descriptions of intervals containing >5 vol% sulfide were carried out on a dedicated sulfide petrology spreadsheet (see “[Sulfide and Oxide Petrology](#),” p. 11). A column for comments is included.
2. The vein/structure spreadsheet (e.g., Table T4) was used to record the presence, apparent orientation, location, width, and mineral content of veins observed on the cut surface of the cores. Each entry records the lithostratigraphic unit and identifiers for the core, section, piece, and the curated depth below seafloor of the top of each piece. For each vein, the location of the top and bottom, depth below seafloor, mineral fillings and proportions, vein width (in millimeters), and apparent orientation of the feature were recorded. The presence or absence of a related alteration halo was recorded by identification of its color, half width (in millimeters), and alteration mineralogy. A column for comments is included (see “[Structural Geology](#),” p. 14, for additional information on core structural measurements).

### Shipboard Geochemical Analyses of Altered Material

Shipboard geochemical analyses on altered rocks collected during Leg 193 were conducted with the ICP-AES using the same suite of elements as that analyzed for fresh igneous rocks (see “[Geochemistry](#),” p. 15). However, except where noted with the data, the analytical methodology differs during sample preparation in one respect. Prior to heating to 1050°C in the furnace, the crushed powder was heated to 600°C and roasted at this temperature for 6 hr to allow oxidation of any sulfide material prior to fusion. All other analytical procedures are identical to those applied to fresh igneous rocks.

---

T2. Abbreviations used in the alteration/mineralization and vein/structure descriptions, p. 62.

---

---

T3. Example of the Alteration/Mineralization Log spreadsheet, p. 63.

---

---

T4. Example of the Vein/Structure Log spreadsheet, p. 64.

---

## X-Ray Diffraction

Bulk-rock XRD analysis was undertaken on a large number of samples to determine the mineralogical composition of altered rocks. Standard XRD operating procedure and conditions were adhered to, and an interactive software package (R. Petschick, Macdiff 3.1, 1995) was used to help identify the main minerals. Minerals are termed major, minor, or trace based on peak height in the XRD spectra. However, peak heights may be strongly influenced by factors other than abundance, so no quantitative measurement is implied. In particular, the abundances of clay and phyllosilicate minerals are not quantitatively estimated and likely to be underestimated.

To provide a semiquantitative estimate of anhydrite abundance, XRD spectra were taken for a number of quartz-anhydrite mixtures of known proportions. The relative peak heights were used to provide a calibration for the estimation of the anhydrite content of quartz-bearing altered rocks. The calibration does not account for the effect of other minerals, and therefore, values should be considered indicative at best.

## Refractive Index Measurements

The RI measurements provided a simple, quick method to distinguish between alteration phases with otherwise similar properties (most notably barite and anhydrite and quartz and cristobalite). The methodology followed was identical to that described in *"Igneous Petrology,"* p. 4. Preliminary petrological observations using crushed particles mounted in oil were used in several instances where quick information was required for description purposes or where thin-section manufacture was impractical or not intended.

## Short-Wave Infrared Spectrometry

During Leg 193, short-wave infrared (SWIR) spectrometry was conducted to aid with the identification of fine-grained alteration minerals and in the delineation of the alteration mineral assemblage. The SWIR spectral range was useful in this alteration study as phyllosilicates, hydroxylated silicates, sulfates, and carbonates all have distinctive spectral patterns in this range. Many members of these mineral groups were encountered in the core.

The analysis was conducted using an Integrated Spectronics PIMA (portable infrared mineral analyzer) II. The PIMA II emits a beam of infrared light onto the sample and measures the intensity of the light reflected in each wavelength interval. Certain minerals preferentially absorb particular wavelengths of light. The spectral signatures generated by the differing positions and intensities of absorption features combine to create an overall absorption pattern for the sample, which may be used diagnostically to qualitatively identify the dominant mineralogy of the sample with respect to the mineral groups mentioned above.

The PIMA II works in the spectral range from 1300 to 2500 nm. Measurements are taken incrementally every 2 nm. A 1-cm<sup>2</sup> area of the core representing each alteration type was analyzed with additional measurements taken of features of interest (e.g., vein selvages and patchy alteration).

All spectral results were recorded in digital format and can be found in the *"Supplementary Materials"* contents list. Each of these files has been named by the hole number followed by a three digit number,

which identifies the order in which the sample was acquired for that hole (e.g., 1188A001.TXT). The first column of the data gives the wavelength (stepped at 2-nm intervals from 1300 to 2500 nm), and the second column records the reflectance intensity (from 0 to 1). All data in these files are tab delimited. An example of this data format is given below.

```
1300  0.715
1302  0.720
1304  0.698
```

Additional data for all the samples are present in the "PIMALOG.TXT" file. This file gives the file name, site, hole, core, section, piece number, and comments for each sample acquired. Specific features are also noted, when analyzed.

### **A Note on the Alteration/Mineralization Logs**

The very fine aphyric nature of the majority of the rocks drilled during Leg 193 made mineral identification and estimation of percentages in hand specimen extremely difficult. In many cases, subsequent examination of thin sections and XRD analyses indicated that the relative proportions of minerals, as estimated in hand specimen, were erroneous. Additionally, as it was necessary to distinguish alteration types based on hand-specimen properties, the three principal types of alteration (bleaching, silicification, and green silica-clay [GSC] alteration) were separated mainly by using color and hardness. An unfortunate side effect of this necessarily simplistic approach was the misidentification of moderately altered volcanic rocks in the lower parts of Holes 1188F and 1189B as completely silicified units, based on hardness.

Because of the time constraints, it was not always possible to correct the alteration logs (see the "[Core Descriptions](#)" contents list) to reflect additional information obtained by more sophisticated methods. In particular, mineral abundances listed on the logs should be considered to be indicative, at best. Thin-section descriptions provide the more reliable estimate of mineral abundances.

## **SULFIDE AND OXIDE PETROLOGY**

Mineralization in seafloor sulfide deposits can occur as massive sulfides, semimassive sulfides, sulfide minerals in stockworks, stringers, or veins, sulfide-filled breccias, disseminated sulfides, Fe-Mn-Si oxide deposits, and metalliferous (sulfide and oxide) sediments. The sulfide or sulfide-bearing rocks are referred to in this report as simply "sulfides" or "sulfide rocks." Any rock containing  $\geq 5\%$  sulfides was regarded to be a sulfide rock. The manner in which they are curated, sampled, described, and analyzed overlaps procedures established for both igneous and hydrothermally altered rock (see "[Hydrothermal Alteration](#)," p. 8, "[Igneous Petrology](#)," p. 4, and "[Geochemistry](#)," p. 15). In addition, for rocks in which the sulfide content was  $< 5\%$ , microscope observations with reflected light of sulfides (and oxides) in polished thin section are described as appropriate.

## Core Curation and Shipboard Sampling

Core pieces were cut with a rock saw. Cores were designated using leg, site, hole, core, section, piece, and core type as discussed in [“Introduction,”](#) p. 1. Each piece was examined for volcanic or relict volcanic features, structural orientation, sulfide and oxide mineralogy, mineral textures, vein distribution, and hydrothermal alteration.

The archive half of each hard-rock sulfide core was described on a cruise-specific form (see “Sulfide Logs” in the [“Core Descriptions”](#) contents list) and was photographed before storage. Photographs (macroscopic, binocular, and microscopic) were taken to illustrate representative structures and textures. During the core description process, samples were selected from the working half for analysis of physical and chemical properties.

We tried to retard the oxidation of sulfide-bearing rocks by sealing them as quickly as possible in nitrogen purged bags, but tattletale oxygen indicators sealed with the cores indicated the storage bags were permeable.

Sulfide-rich samples for shore-based spectroscopic surface analysis were taken before the core was split to avoid oxidation. This sampling was done in conjunction with the microbiological sampling (see [“Microbiology,”](#) p. 19, for further details). Large whole-round pieces were removed from the core and transferred into an anaerobic chamber. The whole-round pieces were split and pristine (expected to be unoxidized) center samples were obtained. The rest of the sample (all outside parts) was returned to the original core for curation.

## Visual Core Descriptions

Sulfide rocks and their alteration phenomena were described using a variant of the standard VCD form for igneous rocks, to which was added a set of symbols for mineralization. All visual descriptions of sulfide rocks were entered into a computerized database (see the “Sulfide Logs” or the “Alteration Logs,” both in the [“Core Descriptions”](#) contents list, for rocks containing <5% sulfides). These forms were completed for each lithologic unit and are described below (see [“Sulfide Description Spreadsheet,”](#) p. 13). More detail was obtained in some instances from examination of polished thin sections as described below (see [“Polished Thin-Section Description,”](#) p. 14).

A classification system was established based on the macroscopic description of the samples. Each rock type is defined by its content of principal minerals, as determined by hand-sample examination and its most prominent textures. The mineral content and textural characteristics of representative samples of each type were confirmed using polished thin-section data. The principal minerals are generally distinguishable macroscopically. Common opaque minerals are pyrite, chalcopyrite, and sphalerite (includes wurtzite). Common nonopaque minerals, referred to as “gangue minerals” by sulfide petrologists, are quartz, silica (which includes cristobalite and amorphous silica), anhydrite, and undifferentiated clay minerals. The opaque mineral magnetite was included with the gangue minerals as part of the alteration assemblage unless it was clearly of igneous origin. Gangue minerals typically fill veins, fractures, pore spaces, and cavities in host volcanic rocks; they also are present as discrete grains disseminated throughout the sulfides or intimately intergrown with sulfides. By convention, ma-

for constituents are  $\geq 10$  vol%, minor constituents are  $\geq 2$  and  $< 10$  vol%, and trace constituents are  $< 2$  vol%.

Determination of sulfide textures is more subjective. Various terms used conventionally by sulfide petrologists are defined in Table T5. The determination of “grain size” refers primarily to the size of discrete minerals or aggregates of intergrown minerals and not to individual grains or crystals within an aggregate. For the purposes of Leg 193 sulfide descriptions, “extremely fine grained” is  $< 0.001$  mm in diameter, “very fine grained” is between 0.001 and 0.5 mm, “fine-grained” is  $> 0.5$  mm to 1 mm, “medium-grained” is  $> 1$  to 2 mm, and “coarse-grained” is  $> 2$  mm (see note on Table T6). Individual crystals, when visible, are described as anhedral, subhedral, or euhedral. Special mention is made of textural relationships between sulfide minerals such as overgrowths, inclusions, and replacements that are the basis for establishing a detailed paragenetic sequence. The term “paragenesis” is taken to mean an assemblage of minerals, whereas “paragenetic sequence” is the order of precipitation of minerals within a given assemblage (Table T7).

The various sulfide types are determined without any particular reference to stratigraphic relationships, and the major characteristics of the different types are summarized in Table T7. This classification system is meant to account only for the sulfide-bearing rocks obtained during Leg 193. Mineralogical and textural features of sulfides found in other sites, including sediment-starved mid-ocean ridges (Leg 158; see Humphris, Herzig, Miller, et al., 1995) and sedimented ridges (Legs 139 and 169; see Davis, Mottl, Fisher, et al., 1992; Fouquet, Zierenberg, Miller, et al., 1998), are mostly different from those observed during Leg 193. Mineral abundances listed in Table T7 are approximate and meant to serve only as a guide for identification of different sulfide rock types. Mineral abundances within individual sulfide types may vary widely.

### Sulfide Description Spreadsheet

Descriptions of mineralized sections containing  $\geq 5\%$  sulfides were summarized on the VCD sheets (see “[Hydrothermal Alteration](#),” p. 8, and “[Geochemistry](#),” p. 15). Detailed descriptions of these mineralized intervals were also entered on “Sulfide Log” spreadsheets (see the “[Core Descriptions](#)” contents list).

As for the other description recording tables used during Leg 193, identifier information is presented for each piece of core described and each line of the spreadsheet represents a separate piece of core or a bay in the core tray. The heading “Mineralization” refers to the proportion of each logged interval that is “mineralized” (i.e., composed of sulfide minerals and associated gangue). Pervasive alteration associated with disseminated mineralization is not considered to be gangue. The “Style” heading refers to the sulfide mineralization styles that are listed in Table T5. Space is then provided to record texture, grain size, and proportion of total mineralized material for individual mineral species, both sulfide and gangue. The textural terms that were used are also listed in Table T5. The percentage of individual minerals was estimated visually from hand specimen, except where additional information was available from polished thin sections or XRD. By convention, the sum of the percent of sulfide and gangue for each interval totals 100%. The “Comments” column was used to record additional information on each sample, including a denotation of intervals sampled for geochemistry or from which polished thin sections were cut.

---

T5. Textural terms and abbreviations used to describe sulfide mineralization, p. 65.

---

---

T6. Grain-size classification for minerals, p. 66.

---

---

T7. Classification of sulfide samples and other hydrothermal precipitates, p. 67.

---

## Polished Thin-Section Descriptions

Most of the cores recovered during Leg 193 contained sulfide minerals and a few were even semimassive sulfides. Polished thin sections of these sulfides were examined to refine visual observations and to document textural patterns and mineral relationships in greater detail. Information about sulfides was recorded on a common microscope description form with igneous petrology and alteration. The following information specific to sulfide minerals was recorded: mineral name, mineral percentages, size, morphology, and general comments. The percentages of individual phases were estimated visually. To avoid subjectivity in determining styles of mineralization, sulfide textures, and grain size, conventional terms were used as defined in Tables T5 and T6. These tables also provide abbreviations for these terms. The terminology for styles and textures of sulfide mineralization is consistent with that used for macroscopic descriptions. The polished thin-section descriptions are included in the “Core Descriptions” contents list.

## STRUCTURAL GEOLOGY

### Measurement of Orientation of Structures in Cores

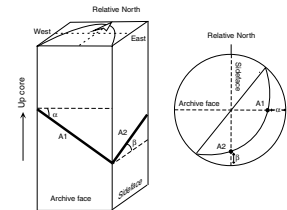
Structural orientations were measured on the archive half of the core using a contact goniometer (Fig. F10). The strike and dip for the plane derived from the two apparent dips was calculated using the geocalculator program in Georient 4.2 (Holcombe, 1996). If the structure could be measured directly, then the strike and dip were entered directly into the vein/structural geology log (Table T8).

### Data Entry

All data were recorded with reference to the structural geology checklist (Table T9) on an ODP standard structural VCD form, of which an example is shown in Figure F11. Data from the descriptions were entered in the structural log (Table T8) under the following headings:

1. Core identifiers: Core, section, piece number, interval, curated depth to top of piece (in mbsf), piece length, oriented piece (yes/no).
2. Structure: Feature measured (fracture, vein, igneous structures, and contacts) and its generation (e.g., V1 to Vn for veins from the earliest to latest in that particular piece of the core and Va to Vx for veins without crosscutting relationships), length (in cm), thickness (in mm), and hosting unit (igneous rock, altered rock, massive sulfide).
3. Structural orientation: Measured and calculated orientation of structures (as explained above) and general orientation (horizontal [H], subhorizontal [Sh], vertical [V], subvertical [Sv], curved [C], irregular [Ir], stockwork [Sw]) (see Table T2 for abbreviations).
4. Mineral infill: Composition of material filling or lining the structure (dominant and secondary) and other minerals. The abbreviations used are those defined in “Hydrothermal Alteration,” p. 8, and “Geochemistry,” p. 15.

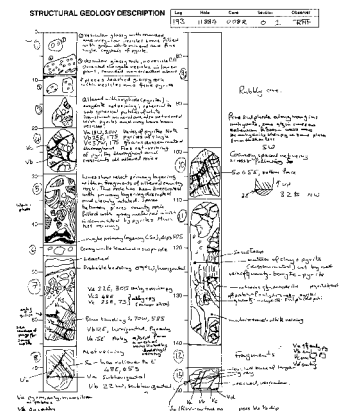
F10. Conventions used during Leg 193 to measure the orientations of structures in cores, p. 49.



T8. Structural log example, p. 68.

T9. Structural geology checklist for descriptions, p. 69.

F11. Example of a structural geology description form, p. 50.



5. *Alteration halo*: Intensity and dominant mineralogy of any alteration halo in wallrock around the measured structural feature.
6. *Comments*: Features that do not fit into any of the other columns.

### Problems in Structural Measurements

Several problems are inherent in any structural study of drilled core. In most cases, only part of the drilled interval in any hole is recovered, and thus, the results are not fully representative. In addition, there may be preferential loss of core because faulted rocks are commonly weaker than the adjacent bedrock and, therefore, may be lost during the drilling.

It is rarely possible to determine the original orientation of the observed structures. The structures initially can only be oriented relative to local reference coordinates based on the orientation in the core tray. The drilling process undoubtedly caused fracturing and rotation of the individual pieces of the core, so this reference orientation may be consistent over only a few tens of centimeters if correlations cannot be made between structures in the separate pieces of the core. Thus, in most instances each piece of core would need to be oriented back to its real position according to an external reference frame, such as by down-hole logging tools and paleomagnetic measurements. This has not yet been attempted.

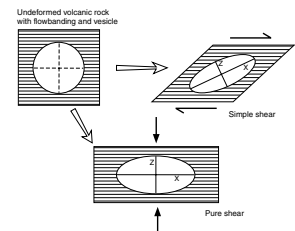
In some pieces of volcanic rocks found throughout the recovered cores, the orientation of elongated flattened and stretched vesicles was used to define the approximate orientation of the volcanic layering. This assumes that flattening of the vesicles is by pure shear alone. Were simple shear involved during flow of these lavas, then the elongation direction of the vesicles would show the approximate orientation of the of the XY plane of the strain ellipsoid in the cut faces of the core (Fig. F12). At high shear strains, however, this would rotate close to the most likely layering orientation. As the vesicles in the cores intersected were generally flattened, albeit tending toward prolate, it was more reasonable that the flattening was by loading normal to and/or shear parallel to the bedding surface of the lava. Therefore, the orientation of the flattening plane of the vesicles was interpreted to give a fair indication of the general orientation of the volcanic layering in the cases where flowbanding was not present.

## GEOCHEMISTRY

### Objectives

Geochemistry during Leg 193 concentrated on the analysis of igneous rocks, altered rocks, and in situ downhole water samples. The analytical methods used were elemental analyses of total nitrogen, carbon, hydrogen, and sulfur in rock samples and ICP-AES analyses of all rock types and waters as well as ion chromatography (IC) of waters. A sulfide methodology for the ICP-AES analyses was developed for digestion and analysis of sulfide samples and is described in "[Geochemistry](#)," p. 65, in the "Site 1188" chapter. Water samples were analyzed for major cation and anion concentrations as well as salinity, alkalinity, temperature, and pH. In addition, the concentration of H<sub>2</sub>O-soluble sulfate of altered rocks was determined gravimetrically.

F12. Relationship between vesicles and flowbanding in a volcanic rock under different shear regimes, p. 51.



## Methods

Before undergoing elemental analysis for carbon, hydrogen, nitrogen, and sulfur and ICP-AES analysis, samples were sawed into small blocks and the saw marks and exterior surfaces (with associated contamination) were removed by grinding on a diamond lap wheel. The sample blocks were subsequently rinsed for 15 min in deionized water, then rinsed again in a methyl alcohol ultrasonic bath for 10 min and subsequently dried at 110°C. The clean blocks were crushed in a Spex 8510 shatter box using tungsten carbide barrels. Whenever recovery permitted, at least 5 cm<sup>3</sup> of material was ground to ensure a representative sample was analyzed. Weighing measurements were made on a Scientech balance with weighing error of ±0.0005 g.

### NCS Elemental Analysis

The samples selected for ICP-AES analysis and splits of the samples selected and prepared for XRD were analyzed on an NA1500 Carlo Erba NCS (nitrogen, carbon, and sulfur) elemental analyzer for total sulfur, nitrogen, hydrogen, and carbon. The sample powders (5 mg) were combusted at 1000°C in an oxygen atmosphere with the addition of vanadium pentoxide to convert sulfur to SO<sub>2</sub>, carbon to CO<sub>2</sub>, and nitrogen to NO<sub>2</sub>. The NO<sub>2</sub> was then reduced to N<sub>2</sub> using copper metal. The gases were separated by gas chromatography and measured with a thermal conductivity detector. The precision of these analyses is better than 1%–2% of the analyzed values of the standards. The total sulfur values were initially used to screen the samples with high sulfur values from those with low sulfur values for method development on the ICP-AES. Total sulfur values were also used in the calculation of the H<sub>2</sub>O-soluble sulfate phase content using the equation:

$$TS = S_{\text{soluble sulfate}} + S_{\text{sulfide + insoluble sulfate}}$$

where TS is total sulfur,  $S_{\text{soluble sulfate}}$  is sulfur in H<sub>2</sub>O-soluble sulfate phases, and  $S_{\text{sulfide + insoluble sulfate}}$  is sulfur in sulfide phases plus H<sub>2</sub>O-insoluble sulfates. The total sulfur values are reported in the tables together with the major element oxide, trace element, and loss on ignition (LOI) data for samples from each site. In general, the values range from trace amounts in the unaltered rocks to 9% TS in the highly altered units. The precision for this method is 1%–2% of the measured quantities. Subsequently, all samples from Hole 1188A were analyzed following the methods for geochemistry described below.

In addition to the rock samples, the residue from the LOI analysis (ignited in quartz crucibles) was also measured on the Carlo Erba NCS elemental analyzer for sulfur contents to check for the extent of oxidation and the removal of sulfur from the samples during ignition. The pre- and post-ignition values obtained for the elemental analysis of total sulfur showed that not all sulfur-bearing components were removed in the LOI roasting process. Because small amounts of barite have been found in thin section and by XRD, it is possible that the residual sulfur in the samples is, in part, attributed to barite, which would not be affected by the LOI temperature of 1050°C. The carbon values are quite low and are ignored because the samples were milled in a tungsten carbide shatter box. Also, no carbonate minerals have been identified in thin section or by XRD. The carbon dioxide component of the LOI is therefore mod-

eled as  $\text{CO}_2 = 0$ . The nitrogen blank was unusually high, potentially because of a small leak in the sample inlet assembly, therefore these data, also generally low values, are also ignored. Hydrogen values from the NCS analysis were used to calculate the  $\text{H}_2\text{O}^+$  content of the samples.

### **ICP-AES**

An ICP-AES instrument (Jobin Yvon JY2000) was used to determine the major oxide and selected trace element abundances of the ignited whole-rock powders. Major oxides and the concentrations for the trace elements Zr, Y, Zn, Cu, Ba, and Sr were determined by ICP-AES analyses following the general procedure outlined by Murray et al. (2000) and Shipboard Scientific Party (2001). Analyses were carried out on lithium metaborate fusions prepared from 100 mg of ignited powder that was mixed with 400 mg of preweighed (on shore) lithium metaborate. This mixture was melted in air at  $1150^\circ\text{C}$  in a Pt-Au crucible for 10 min. The resulting fused bead was cooled, removed from the crucible, and dissolved in 50 ml of nitric acid (2.3 M) during agitation for 1 hr. The 4:1 flux-to-sample ratio was used for samples, standards, and blanks. This reduces the matrix effects for a range of igneous rock compositions. Therefore, the relationship between plasma emission intensity and concentration becomes linear and can be described by

$$C_i = (I_i \cdot m_i) - b_i,$$

where  $C_i$  is the concentration (in either oxide weight percent or parts per million) of element  $i$ ,  $I_i$  is the net peak intensity (in voltage) of element  $i$ ,  $m_i$  is the slope of the calibration curve (in concentration per voltage) for analyte  $i$ , and  $b_i$  is the measured blank of element  $i$  (in either oxide weight percent or parts per million). The slope  $m_i$  was calculated by regressing a line through intensity data obtained by measurement of well-characterized standard reference materials (U.S. Geological Survey STM-1 and RGM-1 and Geological Survey of Japan JA-2, JA-3, JB-2, and JR-2).

### **Methods for Igneous and Sulfide Rock Geochemistry**

Major oxide concentrations, along with a set of six trace elements, were acquired by ICP-AES. Cu and Zn were added to an existing igneous-rock analytical methodology because of their importance in mineralized systems, whereas Zr and Y were included to help assess percentage of the altered rocks and Sr and Ba to help characterize alteration style.

An ICP-AES sulfide method was developed for samples containing >10% total sulfur as sulfides. This involved roasting the samples at  $600^\circ\text{C}$  for 6 hr to oxidize all the expected sulfide sulfur. Subsequently, the oven temperature was raised to  $1050^\circ\text{C}$  and the standard LOI methodology was followed. This two-step heating procedure was employed so as not to damage the quartz crucibles. The fluxing of the samples, and reference rocks, was then completed in ultrapure graphite crucibles. Standard dissolution techniques were used to digest the fused bead into a solution.

## Sulfate Analysis

To obtain the ratio of H<sub>2</sub>O-soluble sulfate to sulfide in the rocks from Holes 1188A and 1189A, a portion of the powdered rock prepared for the ICP-AES analysis was used for a gravimetric sulfate determination. First, 0.5 g of sample was weighed in a 50-mL polyethylene centrifuge tube and then 50 mL of nanopure water (18.2 MΩ) was added. The samples were agitated and then placed in a rack in a 4°C refrigerator for 12 hr. The samples were then centrifuged, and the supernatant liquid was filtered. The filtered solution was transferred to an acid-washed beaker, to which barium chloride was added promoting the precipitation of BaSO<sub>4</sub>. Samples were covered with a watch glass and allowed to react for another 12 hr, after which the barium sulfate was filtered through pre-weighed 0.45-μm filters. The concentration of sulfate in the former solution was determined gravimetrically. The difference between the total sulfur from the elemental analyzer and the gravimetric measurement of soluble sulfate was considered to represent the insoluble sulfide fraction of the sample along with any barite present in the rock.

## Water Samples

Fe, Mn, Ba, Li, and Sr concentrations were determined by ICP-AES analysis following the general procedure outlined by Murray et al. (2000). During Leg 193, given the close proximity of the sites, three water samples were collected over the side of the ship and are suggested to be generally representative of the bulk seawater contribution of the hydrothermal system. Water samples were collected into acid-cleaned plastic buckets from the side of the ship and filtered through sterile 0.45-μm Gelman polysulfone disposable filters. Samples for shipboard analyses were stored in plastic vials and those for shore-based analyses were stored in heat-sealed acid-washed plastic tubes and/or glass vials.

Analyses of water samples followed the procedures outlined by Gieskes et al. (1991). Salinity was measured with a Goldberg optical handheld refractometer. The pH and alkalinity were measured by Gran titration with a Brinkmann pH electrode and a Metrohm autotitrator. The Cl<sup>-</sup> concentration was measured by titration against silver nitrate. Concentrations of NH<sub>4</sub><sup>+</sup> were measured by spectrophotometric methods with a Milton Roy Spectronic 301 spectrophotometer. The concentrations of K<sup>+</sup>, Mg<sup>2+</sup>, Na<sup>+</sup>, Ca<sup>2+</sup>, and SO<sub>4</sub><sup>2-</sup> were measured by ion chromatography using a Dionex DX-120 instrument. Analytical precision was determined by replicate analyses of natural samples and by reanalyzing standards as unknowns. Values of precision (expressed as percent of the measured value) are as follows for the respective constituents: alkalinity is <1.5%; C<sup>-</sup> is 0.4%; Ca<sup>2+</sup> is ~<1%; Mg<sup>2+</sup> is 0.5%; NH<sub>4</sub><sup>+</sup> is ~5%; K<sup>+</sup> is <3%; SO<sub>4</sub><sup>2-</sup> is <4%; and Na<sup>+</sup> is <5%. Chemical data for borehole waters are reported in molar units.

Some rock samples used for porosity measurements (see **“Physical Properties,”** p. 21) yielded such high porosity values that it was hypothesized that soluble sulfate minerals were dissolving during the measurement. To test this, selected rock samples were soaked for 24 hr in seawater, and the water was subsequently analyzed by IC for SO<sub>4</sub><sup>2-</sup> concentration.

## MICROBIOLOGY

The primary microbiology objective for Leg 193 is to establish the nature, extent, and habitat control of microbial activity within the PACMANUS (Papua New Guinea-Australia-Canada-Manus) hydrothermal system. Furthermore, we aim to interpret the differences encountered in the diversity and biomass in terms of the nutrient supplies and environmental habitat in the context of the geochemical and hydrological understanding of the total hydrothermal system.

To achieve these objectives, samples from the core of the hydrothermal system were collected for both shipboard and shore-based studies. Shipboard studies included

1. Determination of abundance and distribution of microorganisms by direct counting fluorescence microscopy,
2. Micromorphological characterization by microscopic observations,
3. Analysis of adenosine triphosphate (ATP) to determine the biomass activity of the subsurface biosphere, and
4. Cultivation of microorganisms at different conditions (thermal and aerobic/anaerobic) for enrichment purposes.

Shore-based studies will include

1. Anaerobic and aerobic culturing,
2. Biochemical typing using specific markers for living and dead microbes,
3. Molecular typing using specific DNA/RNA markers for the classification of microorganisms,
4. Scanning electron microscopic (SEM) techniques, fluorescence and in situ hybridization, and/or other staining procedures to determine the role of microorganisms in mineralization and alteration processes,
5. Transmission electron microscopic (TEM)/atomic force microscopic (AFM) and Fourier transmission infrared spectroscopic (FTIR) studies of the mineral-microbial interaction processes, and
6. Cultivation of microorganisms and analysis for potential bioactive molecules.

Interpretations of shipboard and shore-based results are complicated by the possibility of contamination of samples with microbes from seawater, drilling equipment, and postcollection processing of samples. To minimize the problems of contamination, special handling, sampling, and sample treatment protocols were established. Further, to confirm suitability of the core material for microbiological research, contamination assays were conducted to quantify the intrusion of drill water using perfluorocarbon and fluorescent microsphere tracer procedures.

### Sampling

Whole-round cores or large fragments of the core were collected in the core splitting room immediately after the core liner was split (rotary core barrel [RCB] core) or cores were removed from barrels (ADCB core). The cores were only handled with latex gloves washed with 70% eth-

anol. Following the selection of the appropriate piece and photography by handheld digital camera, the whole-round sample was transferred to the fume hood in the chemistry lab where the outside of the sample was flamed (sterilized) using a torch. Subsequently, the sample was transferred into the anaerobic chamber, equilibrated with an atmosphere containing a mixture of N<sub>2</sub> (90%), CO<sub>2</sub> (5%), and H<sub>2</sub> (5%) usually within 20–30 min of the core arriving on deck. The outer surface of the whole-round core was split off using a hydraulic rock trimmer to minimize transfer of drilling-induced contamination from the outer sample surfaces to the interior of the sample. The remaining parts of the sample (all the outer parts) were returned to the core laboratory for curation.

The pieces selected for shore-based microscopic observations were placed in sterile opaque vessels or vials. Other samples for shore-based studies were fixed in 4% paraformaldehyde or mixed with anaerobic or aerobic media and stored at 4°C or at –70°C, or they were fixed in 4% paraformaldehyde (10% phosphate buffer saline [PBS]) and refrigerated for 2–24 hr, subsequently rinsed with PBS and stored in 1:1 ethanol-PBS at –20°C. Samples for postcruise biochemistry and molecular biology studies were stored in sterile bags at –80°C.

### **Tracer Tests**

To determine potential levels of contamination of samples during drilling, two tracer test systems were used—perfluorocarbon tracer (PFT) and fluorescent microspheres (Smith et al., 2000). Tests were conducted on an average of two to three times for each hole.

## **Shipboard Studies**

### **Abundance and Distribution**

The abundance of subsurface microorganisms was determined by direct fluorescence microscopic counting after 4,6-diamindino-2-phenylindole (DAPI) staining (see below). Such observations can indicate the extent of the deep biosphere. However, it is not possible to determine the activity of the microorganisms from the direct counts, because fluorescent stains can still bind to intact dead cells. For direct counting, a crushed rock sample (1–2 cm<sup>3</sup>) was diluted in 10 mL of filtered-sterilized (0.2 μm) 2% formaldehyde in artificial seawater (FFSW). This solution was vortexed vigorously, and 1 mL was removed with a wide-bore pipet tip, diluted in 10 mL of FFSW, and agitated in a ultrasonic cleaner for 10 min at moderate power. Samples were mixed thoroughly before removing an aliquot for filtration (on preblacked polycarbonate filters—Isopore by Millipore—with a pore size of 0.2 μm and a diameter of 25 mm). The filters were stained with a filtered (0.2 μm) DAPI (0.1 mg/mL final concentration) or with SYBR 1 (Bioprobes). The cells on the filters were examined with a Zeiss fluorescence microscope at 400×–2000× magnification (100× Plan-NEOFLUAR objective) using epifluorescence illumination (100-W Hg bulb) with ultraviolet and blue filter set for DAPI and SYBR 1, respectively. Cells were enumerated and normalized to the volume filtered.

## Biomass Activity Measurements

The ATP concentration extracted from subsurface core samples was measured. The ATP is a biomolecule that serves as a proxy for living biomass and for the source of metabolic energy indicating subsurface bioactivity. The assays were performed in a luminometer (AF-70) using the luciferin-luciferase analysis method (TOA Co., Japan). Crushed rock (1–2 cm<sup>3</sup>) was diluted with 10 mL of 0.5-M trichloroacetic acid solution (TCA; 0.25-M Na<sub>2</sub>HPO<sub>4</sub>) and agitated in an ultrasonic cleaner for 2 min at moderate power. Then, 100 mL of the slurry was transferred to a new vial containing 9.9 mL of N-2-hydroxyethylpiperazine-N-2-ethanesulfonic acid (HEPES) buffer. The diluted sample was transferred again to a new vial and an ATP releasing agent (100 µL) and the luciferin-luciferase solution (100 µL) were added to the vial and mixed. Light production was immediately quantified in the luminometer. Blanks were determined using 100 µL of sterile distilled water, and standards were analyzed using a purified ATP solution. Note, however, that the detection limit of this method is 1.0 fmol ATP/cm<sup>3</sup> (equivalent to 10<sup>4</sup> cells/mL).

## Enrichment Cultivation

Microorganisms were cultured at different thermal and redox conditions. Some microorganisms are believed to be capable of growing at temperatures >100°C, but there is only limited information to address this hypothesis and pressure cells were not available on board. Subsurface samples were incubated at different temperatures using culture media for anaerobic and aerobic bacteria to try to enrich viable microbial populations from the core samples. The media used was of seawater composition (Table T10), and culturing was conducted in air-tight 100-mL serum bottles. The anaerobic media were reduced with cysteine or sodium sulfide, whereas sulfate or bicarbonate was added as an electron acceptor. Electron donors were organic carbon sources such as yeast extract and peptone. Approximately 1 cm<sup>3</sup> of crushed rocks or rock chips were added to the aerobic and anaerobic culture media, respectively. The bottles were incubated at 4°, 25°, 60°, and 90°C. Growth was verified by the accumulation of microbial cells or by metabolic products as seen by increased turbidity.

---

T10. Aerobic and anaerobic cultivation media, p. 70.

---

## PHYSICAL PROPERTIES

Shipboard physical properties measurements provide quantitative information about the composition and lithology of core material and may be used to correlate core data with wireline logging data. All physical properties measurements were taken on the cores after allowing them to equilibrate to room temperature (~25°C). Magnetic susceptibility and natural gamma radiation were measured on whole cores with half liners using the MST. After the cores were split, half-space thermal conductivity measurements were taken on the archive halves of the core. Compressional wave velocity was measured on discrete core samples in one direction. Because no soft sediment was obtained, shear strength was not measured, and only the contact probe system was used in velocity measurements. Finally, wet and dry masses and dry volumes were determined, and water content, bulk density, dry density, grain density, porosity, and void ratio were calculated.

## MST Measurements

The MST has four physical properties sensors—magnetic susceptibility meter (MSM), gamma-ray attenuation (GRA) densitometer, compressional wave logger (PWL), and natural gamma-radiation (NGR) detector. The quality of the measurements is degraded if the core liner is only partially filled or if the core is disturbed. Because this was the case for many of the cores, the GRA densitometer and PWL were not used. However, the remaining tests were completed on all of the cores that were not extensively fragmented, incomplete, or disturbed, because even inaccurate data can be useful in correlating the cores to well log data and understanding rock property trends. Regardless of the inaccuracies, magnetic susceptibility and NGR values are accessible on the Janus database.

Magnetic susceptibility is the degree to which a material can be magnetized in an external magnetic field. It can be used to help detect variations in magnetic properties caused by lithologic changes or alteration. Tests were run at 2-cm intervals using the 1.0-s integration time range on the Bartington meter (model MS2C), which has an 88-mm coil diameter. Most of the cores were composed of small rock fragments that did not fill the core liner completely. Because of the lower-than-ideal volume, values reported in each chapter generally underestimate the magnetic susceptibility. The data were primarily collected to indicate magnetic trends throughout the core as opposed to gathering exact magnetic susceptibility values. To remove the most inaccurate data, a 0.5-cm interval on either side of the rock fragment dividers was not measured.

The NGR measures the discrete decay of  $^{40}\text{K}$ ,  $^{232}\text{Th}$ , and  $^{238}\text{U}$ , which are three long-period isotopes that decay at essentially constant rates within measurable time scales. The operation principles of the NGR system are outlined by Hoppie et al. (1994). Natural gamma-ray emissions were measured every 15 cm on the core for a 30-s interval. The NGR system was calibrated in transit against a thorium source, and sample standards were measured at the end of operations for every site. Similar to the MSM measurements, the quality of NGR measurements is compromised because of the incoherent and incomplete nature of the cores. Again, the data primarily serve as an indicator of where natural gamma-ray emissions are present.

## Thermal Conductivity

Thermal conductivity is the measure of the rate at which heat flows through a material. It is dependent on the composition, porosity, density, and structure of a material. Thermal conductivity was measured through transient heating of the core with a known heating power and a known geometry and recording the change in temperature with time, using the TK04 system described by Blum (1997). Measurements were made in half-space mode (Vacquier, 1985) at an interval of at least one per lithologic unit. The half-space determinations were made by placing a needle probe in a grooved epoxy block with a relatively low conductivity (Sass et al., 1984; Vacquier, 1985) onto a flat surface of the sample. The measurements were conducted in a seawater bath to keep the samples saturated, to improve the thermal contact between the needle and the sample, and to reduce thermal drift. All samples were allowed to equilibrate to the water temperature before tests were run. At the beginning of each measurement, the TK04 system conducts a self

test for calibration. If temperature variations during the test are too high, the test aborts. Data are reported in W/(m·K) units. For each thermal conductivity data point reported, the thermal conductivity was measured at least three times and the values were averaged. If variability was large, additional measurements were taken until consistent values were obtained. Only the consistent measurements were used in the averaged value. If no consistent values could be obtained, the data for that sample were discarded. Thermal conductivity measurements made on a standard of known value were conducted periodically during the cruise to test the accuracy of the system. Measurements were always within 0.05 W/(m·K) of the known value, which is smaller than the analytical uncertainty of the instrument (5%; Blum, 1997). Individual thermal conductivity measurements as well as averaged values are accessible on the Janus database.

### **Compressional Wave Velocity**

Discrete compressional wave velocity measurements were made using the contact probe system (PWS3) with a frequency signal of 500 kHz. Measurements were made approximately once per core in one direction. The core was sampled as 2.54-cm minicores drilled perpendicular to the core. No measurements were made for velocity anisotropy. The top and bottom of each minicore were cut to be parallel to each other and then were polished to improve coupling at the transducer/core interface. Distilled water was applied to the top and bottom transducer to improve the coupling as well.

### **Index Properties Measurements**

Minicores were sampled from each lithologic unit where possible. When heterogeneity within a lithologic unit was larger than the scale of a minicore (2.54 cm) or when recovered sections were extremely fragmented, rock fragments were taken in one or more places from the unit to obtain a representative sample. When possible, both minicores and rock fragment samples were taken. In rare cases, the recovery of a particular lithologic unit was too small or unsuitable for index properties sampling.

Wet and dry sample masses and dry volumes were measured and used to calculate water content, bulk density, dry density, grain density, porosity, and void ratio. Sample mass was determined using two Scitech electronic balances. The balances were equipped with a computerized averaging system that corrected for ship accelerations. The sample mass was counterbalanced by a known mass such that the mass differentials were generally <1 g. Sample volumes were measured at least three times, or until consistent readings were obtained, using a helium-displacement Quantachrome Penta-Pycnometer. Instrument accuracy is within 0.1% of the measured mass and within 1% of the measured volume (Blum, 1997). A standard reference volume was included with each group of samples during the measurements and rotated among the cells to check for instrument drift and systematic error. Samples were soaked in seawater for 24 hr before determining wet mass. After the 24-hr soaking period, IC measurements of sulfate content in the seawater used for soaking were conducted to measure the amount of dissolution of anhydrite from the minicore samples. In all cases, the amount of mass lost from the sample was insignificant (<0.02% of sample) as compared to the total sample mass. Then samples were oven-dried at  $105^{\circ} \pm 5^{\circ}\text{C}$  for

24 hr and allowed to cool in a desiccator before measuring dry weights and volumes (Method C in Blum, 1997). The following relationships can be computed from the two mass measurements and dry volume measurements (taken from Blum, 1997). When beakers were used, their mass and volume, which are determined periodically and stored in ODP's computer database, were subtracted from the measured total mass and volume. All measured and calculated values are accessible in the Janus database. The directly measured values are

$M_b$  = bulk mass,  
 $M_d$  = dry mass (mass of solids,  $M_s$ , plus mass of residual salt), and  
 $V_d$  = dry volume (volume of solids,  $V_s$ , plus volume of residual salt,  $V_{salt}$ ).

Variations in pore-water salinity ( $s$ ), and density ( $\rho_{pw}$ ), that typically occur in marine sediments do not affect the calculations significantly, and standard seawater values at laboratory conditions were used:

$s = 0.035$  and  
 $\rho_{pw} = 1.024 \text{ g/cm}^3$ .

Pore-water mass ( $M_{pw}$ ), mass of solids ( $M_s$ ), and pore-water volume ( $V_{pw}$ ) can then be calculated:

$$M_{pw} = (M_b - M_d)/(1 - s),$$

$$M_s = M_b - M_{pw} = (M_d - s \cdot M_b)/(1 - s), \text{ and}$$

$$V_{pw} = M_{pw}/\rho_{pw} = (M_b - M_d)/[(1 - s)\rho_{pw}].$$

Additional parameters required are the mass and volume of salt ( $M_{salt}$  and  $V_{salt}$ , respectively) to account for the phase change of pore-water salt during drying (It should be kept in mind that for practical purposes the mass of salt is the same in solution and as a precipitate, whereas the volume of salt in solution is negligible.):

$$M_{salt} = M_{pw} - (M_b - M_d) = (M_b - M_d)s/(1 - s) \text{ and}$$

$$V_{salt} = M_{salt}/\rho_{salt} = [(M_b - M_d) s/(1 - s)] / \rho_{salt},$$

where the salt density ( $\rho_{salt} = 2.20 \text{ g/cm}^3$ ) is a calculated value for average seawater salt.

Moisture content is the pore-water mass expressed either as a percentage of wet bulk mass or as a percentage of the mass of salt-corrected solids:

$$W_b = M_{pw}/M_b = (M_b - M_d)/M_b(1 - s) \text{ and}$$

$$W_s = M_{pw}/M_s = (M_b - M_d)/(M_d - s \cdot M_b).$$

Calculations of the volume of solids and bulk volume are as follows:

$$V_s = V_d - V_{salt} \text{ and}$$

$$V_b = V_s + V_{pw}$$

Bulk density ( $\rho_b$ ), density of solids or grain density ( $\rho_s$ ), dry density ( $\rho_d$ ), porosity ( $P$ ), and void ratio ( $e$ ) are then calculated according to the following equations:

$$\rho_b = M_b/V_b,$$

$$\rho_s = M_s/V_s,$$

$$\rho_d = M_s/V_b,$$

$$P = V_{pw}/V_b, \text{ and}$$

$$e = V_{pw}/V_s.$$

## ROCK MAGNETISM

The rock magnetic analyses conducted onboard the *JOIDES Resolution* during Leg 193 consisted of continuous pass-through measurements on both whole and split cores and discrete measurements on minicore samples taken from the working half of the split cores. Once a section of the core containing recovered material was brought into the lab, magnetic susceptibility was measured on the whole core before it was split. This was done using the susceptibility meter mounted on the multisensor track (MST). After splitting the core, natural remanent magnetization (NRM) and magnetic susceptibility were measured on the archive half by passing it through the cryogenic magnetometer. Similarly, NRM and susceptibility were measured on discrete rock samples from the working half. One or more 2.5-cm-diameter minicores were generally taken from each lithologic unit recovered for detailed shipboard analyses. An effort was made to select the samples near important structural features and between lithologic boundaries for possible reorientation using the remanent magnetization direction. Stepwise alternating field (AF) demagnetization was conducted on the archive halves of the cores and on discrete samples to isolate stable components of remanence. The discrete samples were imparted with isothermal remanent magnetization (IRM) using a pulse magnetizer. This was done at increasing field strengths while we monitored the changes in IRM intensity. Once the samples became saturated, they were then thermally demagnetized to study the characteristics of their primary magnetic carrier. The results of the magnetic properties were compared with lithologic units and geological features.

### Laboratory Instruments

The remanent magnetization of archive halves and discrete samples from working halves was measured using a 2G Enterprises pass-through cryogenic super-conducting quantum interference device (DC-SQUID) rock magnetometer (model 760R). This pass-through cryogenic magnetometer has an in-line AF demagnetizer (2G model 2G600) that allows for demagnetization of samples up to peak fields of 80 mT. The practical limit on the resolution of natural remanence of core samples is imposed by the magnetization of the core liner itself (~0.01 mA/m). The magne-

tometer and AF demagnetizer are interfaced to a PC-compatible computer and controlled by the 2G Long Core software written using LabVIEW by National Instruments. For many samples, the IRM intensity proved to be too high to be measured by the cryogenic magnetometer. For stepwise demagnetization of discrete samples, the laboratory is equipped with an AF demagnetizer (model D-2000 by DTech Inc.) and a thermal demagnetizer (model TSD-1 by the Schonstedt Instrument Co.) capable of demagnetizing specimens up to 200 mT and 700°C, respectively. An Analytical Services Company (ASC) model IM-10 impulse magnetizer (capable of generating pulsed fields from 0.02 T to 1.35 T) and a PARM-2 system by DTech Inc. were used for IRM acquisition studies of discrete samples.

Whole-core magnetic susceptibility ( $k$ ) was measured at 2-cm intervals using the Bartington Instrument susceptibility meter (model MS1) attached to the MST (see “Physical Properties,” p. 21). The susceptibility data were stored in the Janus database as raw data in units of  $10^{-5}$  SI. The true SI volume of susceptibilities should be multiplied by a correction factor to account for the volume of material that passed through the coils. The standard correction factor for ODP core is  $\sim 0.66$ . Since the susceptibility measurements of the whole core were made following the establishment of the final curated positions and placement of spacers, they are directly comparable with the pass-through measurements on the archive half cores.

The magnetic susceptibility of archive half cores was measured using the archive multisensor track (AMST). Because most of the core samples recovered during Leg 193 were relatively short in length, rather than taking continuous measurements, the AMST was used to take intermittent measurements. Both the MST and the AMST employ the same type of susceptibility meter (Bartington Instruments model MS2), but with a different sensor. The sensor for whole-core measurements (MS2C) is a loop with an 88-mm inner diameter, and the core passes through the sensor coil. The AMST has a cylindrical tip probe (MS2F), and the sensor provides a depth of investigation approximately equal to its diameter (20 mm). The volume susceptibility of the minicores was measured using the Geofyzika Brno Kappabridge KLY-2 magnetic susceptibility meter. The susceptibility values on the Kappabridge are reported relative to a nominal volume of  $10 \text{ cm}^3$ .

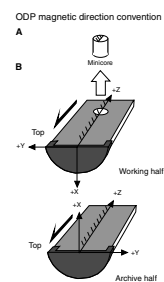
### Sampling Coordinates

The standard ODP core orientation convention (fig. 8, Shipboard Scientific Party, 1991; fig. 8, Shipboard Scientific Party, 1997) was adopted for rock magnetic work during Leg 193. According to this convention, the z-axis is downhole parallel to the core, and the x-axis forms a line perpendicular to the split face of the core and is directed into the working half (Fig. F13). The x-axis is used as the reference “geomagnetic north” for the definition of magnetic declination values. Discrete minicores were marked with an arrow in the negative-z (uphole) direction on the plane representing the split surface of the working half. The plane marked with the arrow is the y-z plane.

### Sampling Method

Cylindrical minicores ( $12 \text{ cm}^3$ ) were extracted from the cores recovered during Leg 193 using a water-cooled nonmagnetic drill bit attached to a standard drill press. Minicores were marked with an arrow

F13. Orientation convention for ODP cores and discrete samples, p. 52.



pointing in the uphole direction. We tried to collect at least one or two discrete samples from each section of the core, and a few samples were used for onboard pilot demagnetization studies.

### Measurements

NRM measurements were taken on the archive half of the core using the cryogenic magnetometer at 2-cm intervals when continuous pieces longer than 15 cm were available. To isolate characteristic magnetization, archive halves were AF demagnetized at 5, 10, 15, 20, and 30 mT. Minicore samples taken from the working half were examined in greater detail. First, we measured the dimensions of the minicore samples. The anisotropy of magnetic susceptibility (AMS) was determined for the samples using the Kappabridge and the program ANI20 supplied by Geofyzika Brno. A 15-position measurement scheme was employed to obtain the susceptibility tensor ( $k_{ij}$ ) from which the associated eigenvectors and eigenvalues were derived. We then measured the NRM of the samples using the cryogenic magnetometer. The samples were AF demagnetized at 10, 15, 20, 25, 30, 40, 50, 60, and 80 mT. The characteristic remanent magnetization was derived using principal component analysis (Kirschvink, 1980). Both Zijderveld (1967) plots and equal-area stereographic projections were used to determine the stability of remanence levels within the archive cores and the discrete samples. The volume susceptibility in conjunction with the NRM intensity was used to estimate the Koenigsberger ratio ( $Q$ , the ratio of remanent to induced magnetization) of the samples. Koenigsberger ratios can be calculated using the following equation:  $Q = J_o \mu_o / kH$ , where  $J_o$  is the NRM intensity,  $\mu_o$  is the permeability of free space ( $4\pi \times 10^{-7}$  H/m),  $k$  is the susceptibility, and  $H$  is the ambient geomagnetic field at the site, which according to IGRF is 36.508 mT. The results from the remanent magnetization and low-field susceptibility measurements were compared with lithologic units and other geologic structures.

For rock magnetic properties measurements, the minicore samples were subjected to stepwise IRM acquisition experiments. The IRM acquisition experiments (to a peak field of 1.2 T) were performed using the ASC impulse magnetometer (model IM-10). After each impulse field step, we measured the remanence of the sample using the cryogenic magnetometer. Many of the IRM values were too high for the cryogenic magnetometer to measure accurately. As a result, the IRM at high field very often exhibited large fluctuations with increasing field strength. To examine the thermal demagnetization characteristics, a number of minicores were progressively heated from 100° to more than 600°C. This was done by heating the sample to a prescribed temperature, allowing the sample to cool back to the room temperature inside the cooling chamber (model TSD-1 by the Schonstedt Instrument Co.), and then measuring the magnetization intensity using the cryogenic magnetometer. Together with the information on the Curie temperature of different magnetic minerals, we were able to identify the dominant magnetic mineralogy of some of the minicores.

## DOWNHOLE MEASUREMENTS

Downhole measurements are used to determine physical, chemical, and structural properties of formations penetrated by a drill hole. Using a variety of instruments, these measurements are rapidly collected to

make continuous in-situ records as a function of depth after the hole has been drilled or reentered. Logs are essential for performing stratigraphic and lithologic characterizations, as well as for determining physical and chemical properties of the formation at a scale that links discrete laboratory measurements with regional geophysical studies. Especially where core recovery is incomplete, logging data may provide the only way to interpret structure and lithostratigraphy. This proved especially valuable during Leg 193 and will continue to be important in the postcruise studies.

Adhering to standard wireline logging techniques, after completion of coring operations the logging tools are combined and stacked together, lowered downhole and pulled up at constant speed while on recording mode. In a somewhat different approach known as logging while drilling (LWD), logging sensors are placed at close proximity to the drill bit and measurements are made while the hole is drilled. However, in this case no core is obtained and the LWD logs are interpreted and correlated to nearby wireline logs and core data. The LWD technique was used during Leg 193 to provide data from the top 60–100 m normally missing from wireline logs in cored holes. The first hard-rock application of both technologies to the same interval in ODP history was performed during Leg 193.

Overall, the quality of logging data is largely determined by the state of the borehole wall. Good contact with the borehole walls is essential for obtaining high resolution data. However, deep investigation measurements such as resistivity and sonic velocity are less sensitive to variations in hole diameter. High temperatures can also limit data quality. During Leg 193, we drilled into a hydrothermal environment that required monitoring of in-situ temperature before running other logs because most logging tools are limited to operational temperatures of 175°C. The logging tools used during Leg 193 are listed in Tables T11 and T12.

### **Memory Tools**

Two types of memory tools were used during Leg 193 to determine downhole temperature conditions. They are listed below. In addition, two glass maximum-reading mercury thermometers were on several occasions attached to the wireline cable head.

#### **Core Barrel Temperature Tool**

The core barrel temperature tool (CBTT) was developed by the Borehole Research Group of the Lamont-Doherty Earth Observatory (LDEO) for assessing temperature conditions while drilling and determining if the conditions were favorable for subsequent LWD operations in hydrothermal environments. Similar to the drill string accelerometer (DSA), the CBTT is another step in a series of measurements while coring that has been used in the past to characterize in situ drilling conditions (Plank, Ludden, Escutia, et al., 2000; Shipboard Scientific Party, 2001). The primary purpose of the CBTT was to measure and record the borehole temperatures while drilling. These measurements could then be correlated to pump rates used during coring operations to determine the feasibility of performing LWD operations in the high temperature conditions that were encountered in the Manus Basin. The CBTT contains a thermocouple and a battery operated electronics board encased

---

T11. Tool strings, special tools, and log acronyms, p. 71.

---

---

T12. Wireline tool strings and properties measured, p. 72.

---

in a single dewar inside the pressure case that was designed for the DSA (Fig. F14).

During Leg 193, the preliminary plan was to use the CBTT in every other core barrel at Sites 1188, 1189, and 1190. The CBTT would be deployed on an RCB core barrel for a mudline measurement and then on every other RCB core barrel run. On each run, the CBTT would begin data acquisition at a predetermined depth as programmed by the logging scientists. For ease of deployment, the CBTT was designed as a removable extension of the RCB core barrel. Using standard threaded connections, the CBTT was attached to the top of the core barrel by a Transocean Sedco Forex core technician prior to the core barrel deployment. Except for the connection and disconnection of the CBTT, coring activities were not affected by its presence. Upon CBTT/core barrel retrieval, the CBTT was disconnected and the data downloaded to the third-party data acquisition system in the Downhole Measurements Laboratory for immediate analysis. The data was then correlated to pumping rates to determine the necessary parameters for successful subsequent LWD operation at Sites 1188, 1189, and 1190. Oven tests performed at LDEO showed that a glycerin-filled dewar allowed the electronics to survive in a 250°C environment an additional 4 hr (Fig. F15). When high temperatures were expected or when temperature conditions were unknown, we planned to use a glycerin-filled dewar to avoid damaging the tool.

### Ultra High Temperature Multisensor Memory Tool

The ultra high temperature multisensor memory tool (UHT-MSM) is a slimhole probe running on the coring line. It was deployed for the first time during Leg 169 (Shipboard Scientific Party, 1998). The tool was developed for the University of Miami by Geophysical Research Corporation (GRC, 1994a, 1994b, 1996). The tool is shown schematically in Fig. F16. The UHT-MSM contains internal and ultra high external temperature measuring devices, a pressure gauge, a multisensor memory unit, and a dewar flask that acts as an insulator to maintain a stable temperature and cool-down rate for the tool (Fig. F16). The heat shield is aircraft-grade aluminum bound at both ends by brass heat sinks. The dewar flask can maintain an internal temperature suitable for tool operation for 4–5 hr at an external temperature of 400°C. Operations are possible up to 10 hr if the average temperature does not exceed 232°C (GRC, 1994a, 1994b) (Table T12).

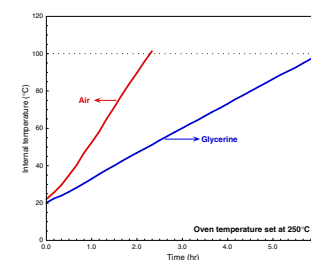
### Wireline Tool Strings

Two combinations of wireline tools were used during Leg 193, the triple combination tool string (triple combo) and the Formation MicroScanner (FMS)/sonic tool strings (Fig. F17). The triple combo measures formation electrical resistivity, density, hydrogen content, and natural radioactivity. The FMS/sonic tool string provides electrical images of the borehole wall and measures acoustic velocity, magnetic field, and natural radioactivity. Natural radioactivity is measured with both tool strings because the data generated are used usually for depth matching between different logging runs. Both tool strings were modified for high-temperature operations by including a high-temperature cartridge that provided additional gamma-ray measurements and real time temperatures of the borehole fluids.

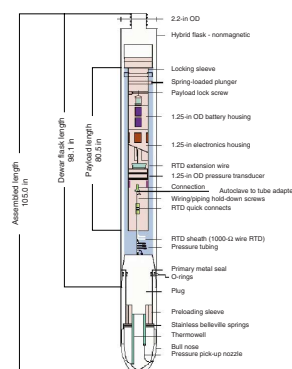
F14. Steps for assembling the core barrel temperature tool, p. 53.



F15. CBTT tests showing the effectiveness of the insulating properties of the dewar system, p. 54.



F16. Schematic diagram showing the major components of the UHT-MSM tool, p. 55.



In the following sections, the basic principle of each tool is summarized. More information about the tools, the type of measurements, and their resolutions is available in Serra (1984), Ellis (1987), Schlumberger (1989), Rider (1996), and in Tables T11 and T12.

## Natural Radioactivity Measurements

Three spectral gamma-ray tools were used to measure natural radioactivity in the formation: the natural gamma-ray tool (NGT), the hostile-environment natural gamma-ray sonde (HNGS), and the high-pressure, high-temperature telemetry gamma-ray cartridge (HTGC).

The NGT uses a sodium iodide (NaI) scintillation detector and 5-window spectroscopy to determine concentrations of potassium ( $^{40}\text{K}$ ), thorium ( $^{232}\text{Th}$ ), and uranium ( $^{238}\text{U}$ ), the three elements whose isotopes dominate the natural radiation spectrum. The HNGS is similar to the NGT, but it uses two bismuth germanate (BGO) scintillation detectors and 256-window spectroscopy for a significantly improved tool precision. The HNGS derives its name from the fact that it is rated to a much higher temperature ( $260^\circ\text{C}$ ) than the NGT ( $175^\circ\text{C}$ ). The BGO crystals provide a significantly better spectral response than the NaI detectors because of their enhanced ability to stop gamma rays and convert their energy to full amplitude signals. This is caused by both their higher density, as compared to the NaI crystals, and their higher atomic number. However, the resolution of the peaks in the spectra obtained by the BGO detectors is not as good as that obtained by the NaI detectors, because the light emitted per unit of deposited gamma-ray energy is only ~12% of what is produced by the NaI crystals.

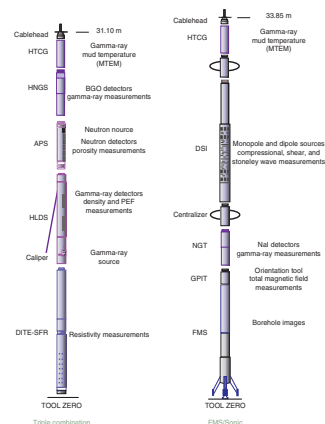
The HTGC has a gamma-ray detector that is made of a NaI crystal, a photo multiplier tube, a high-voltage generation circuit, and a preamplifier of the gamma-ray pulse all built in one package. The number of the output pulses from the detector is counted at a rate of 8 Hz, and the count is sent uphole. Housed in a heatsink and dewar flask that allows operations in high-temperature environments ( $260^\circ\text{C}$ ), this tool also has a 31-pin upper and lower head asset and is combinable with any standard 3.375-in tool without additional adaptors. The data acquisition software cannot distinguish between the tools, but the HTGC has the correct length and measure point and gamma-ray response for the flaked tool.

The gamma-ray values are measured in American Petroleum Institute (API) units. These units are derived from the primary Schlumberger calibration test facility in Houston, Texas, where a calibration standard is used to normalize each tool. Because the natural gamma-ray response is sensitive to borehole diameter and the weight and concentration of bentonite or potassium-chloride present in the drilling mud, corrections are routinely made for these effects during data processing at LDEO.

## Density Measurements

Formation density was measured from gamma-ray attenuation with the hostile environment litho-density sonde (HLDS). The sonde contains a radioactive cesium ( $^{137}\text{Cs}$ ) gamma-ray source (622 keV) and far and near gamma-ray detectors mounted on a shielded skid, which is pressed against the borehole wall by a hydraulically activated arm. Gamma rays emitted by the source experience Compton scattering, which involves the transfer of energy from gamma rays to electrons in

F17. Schematic diagram of the triple combination and FMS/sonic tool strings, p. 56.



the formation via elastic collision. The number of scattered gamma rays that reach the detectors is related to the density of electrons in the formation, which is in turn related to bulk density. Porosity may be derived from this bulk density if the matrix density is known. Photoelectric absorption occurs when gamma rays reach energies <150 keV after being repeatedly scattered by electrons in the formation. Because photoelectric absorption is strongly dependent on the mean atomic number of the elements in the formation, it varies according to chemical composition and is essentially independent of porosity.

### **Hydrogen Content/Neutron Measurements**

The hydrogen content of the formation was measured with the accelerator porosity sonde. The sonde incorporates a minitron neutron generator, which produces fast (14.4 MeV) neutrons, and five neutron detectors (four epithermal and one thermal) that measure the number and arrival times of neutrons at different distances from the source. Neutrons emitted from the source are slowed by collisions with nuclei in the formation, experiencing an energy loss that depends on the relative mass of the nuclei with which the neutrons collide. Maximal energy loss occurs when a neutron strikes a hydrogen nucleus. In sediments, hydrogen is mainly present in pore water, so the neutron log is essentially a measure of porosity, assuming pore-fluid saturation. However, in igneous and hydrothermally altered rocks, hydrogen may also be present in alteration minerals such as clays; therefore, neutron logs may not give accurate estimates of porosity in these rocks.

### **Electrical Resistivity Measurements**

The electrical resistivity of the formation was measured with the dual induction tool-phasor (DIT-E). This sonde provides three measures of electrical resistivity based on different depths of investigation—shallow or spherically focused log (SFL), medium (IMPH), and deep (IDPH).

The DIT-E provides two inductive measurements, IDPH and IMPH. An alternating current of high frequency and constant intensity is sent through a transmitter coil. This current induces an alternating magnetic field, which again induces currents in the formation flowing in circular ground loops. These currents create, in turn, a magnetic field which induces a voltage in the receiver coil. Both the IDPH and IMPH are commonly used to evaluate the formation properties away from shallow borehole disturbances that could have been created by drilling processes.

The SFL provides a galvanic measurement of electrical resistivity with shallow penetration but high vertical resolution. A bucking current system establishes equipotential spheres. An independent survey current flows through the volume of investigation. Its intensity is proportional to the formation conductivity.

### **Sonic Measurements**

Sonic velocities were measured with the dipole shear imager (DSI). The DSI employs a combination of monopole and dipole transducers to make accurate measurements of sonic wave propagation in a wide variety of lithologies (Schlumberger, 1995). In addition to compressional wave velocity measurements, the DSI excites a flexural mode in the borehole, which can be used to determine shear wave velocity in all

types of formations. The configuration of the DSI also allows recording of cross-line dipole waveforms, which can be used to estimate shear wave splitting caused by preferred mineral and/or structural orientations in consolidated formations. A low-frequency source enables Stoneley waveforms to be acquired as well. These “guided” waves are associated with the solid/fluid boundary at the borehole wall and their amplitude exponentially decays away from the boundary in both the fluid and the formation.

### Temperature Measurements

The HTGC also has an external sensor that allows for real time temperature measurements of the borehole fluids. This sensor was located on the cablehead that was used on top of both the triple combo and the FMS/sonic tools strings. Two thermocouples were used to calibrate the cablehead temperature measurements. At 0°C there is a -1.1°C difference between the calibration standard and the cablehead measurements. At 106°C there is a 1.7°C difference (Fig. F18).

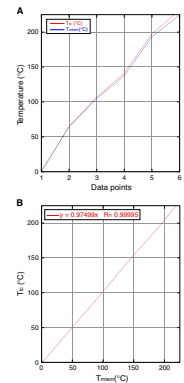
### Logging While Drilling

During Leg 193, the Anadrill resistivity-at-the-bit (RAB) tool was deployed. The tool provides resistivity measurements and electrical images of the borehole wall, similar to the FMS but with complete coverage of the borehole walls and slightly lower vertical resolution (Table T12). In addition, the RAB tool contains a scintillation detector giving a total gamma-ray measurement. A caliper log is not available from RAB measurements; thus, the shape of the borehole is not known and the influence of breakouts on the log responses cannot be estimated.

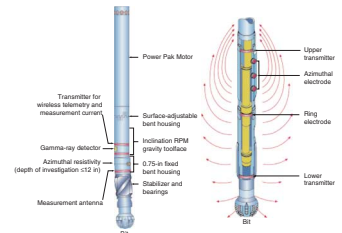
The RAB tool is connected directly to the drilling bit and uses the lower portion of the tool and the bit as a measuring electrode (Fig. F19). This allows the tool to provide a bit resistivity measurement with a vertical resolution just a few inches longer than the length of the bit. A 1.5-in electrode is located 3 ft from the bottom of the tool and provides a focused lateral resistivity measurement ( $R_{RING}$ ) with a vertical resolution of 2 in. The characteristics of  $R_{RING}$  are independent of where the RAB tool is placed in the bottom-hole assembly (BHA) and the  $R_{RING}$  depth of investigation is ~22 in. In addition, button electrodes provide shallow, medium, and deep resistivity measurements as well as azimuthally oriented images. These images can then reveal information about formation structure and lithologic contacts. The ~1-in-diameter button electrodes reside on a clamp-on sleeve, which limits borehole wall standoff in an 8.5-in borehole to 0.188 in. The buttons are longitudinally spaced along the RAB tool to render staggered depths of investigation of ~11, 15, and 19 in. The tool’s orientation system uses the Earth’s magnetic field as a reference to determine the tool position with respect to the borehole as the drill string rotates thus allowing both azimuthal resistivity and gamma measurements. Furthermore, these measurements are acquired as the RAB rotates, with an ~6° resolution.

The RAB collar configuration is intended to run in 8.5- and 9.875-in holes depending on the measuring button sleeve size. Although only an 8.25-in measuring sleeve was on board during Leg 193, both 8.5- and 9.875-in BHA configurations for the RAB tool were available (Fig. F20). Using an 8.5-in bit and 6.75-in collar configuration provides a shorter standoff between the resistivity buttons and the formation (~0.25 in)

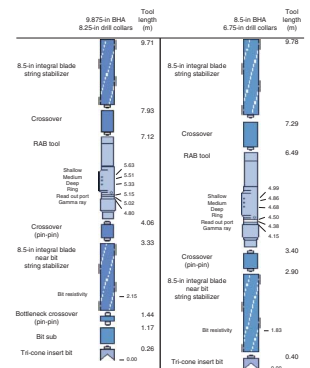
F18. Calibration performed for the MTEM sensor at the Schlumberger Offshore Division facilities in Houston, p. 57.



F19. Schematic diagram of the RAB tool, p. 58.



F20. Schematic diagram of the RAB tool and the BHA, p. 59.



and higher resolution images; whereas the larger bit assembly provides more stability when beginning a hole in difficult drilling environments. During Leg 193, the 9.875-in assembly was used because of concerns in starting a hole with the smaller diameter collars.

## RAB Tool Specifications

### Resistivity Measurements at the Bit ( $R_{\text{BIT}}$ )

For the RAB measurement, a lower transmitter produces a current and a monitoring electrode located directly below the ring electrode measures the current returning to the collar. When connected directly to the bit, the RAB tool uses its lower few inches and the bit as a measuring electrode. The resultant resistivity measurement is termed  $R_{\text{BIT}}$ . When transmitted to the surface in real time,  $R_{\text{BIT}}$  gives the most immediate information about the formation.

### Ring Resistivity Measurements ( $R_{\text{RING}}$ )

The upper and lower transmitters produce currents in the collar that meet at the ring electrode. The sum of these currents is then focused radially into the formation. These current patterns can become distorted depending on the strength of the fields produced by the transmitters and the formation around the collar. Therefore, the RAB tool uses a cylindrical focusing technique that takes measurements in the central monitor coil and a lower monitor coil to reduce distortion and create an improved ring response. The ring electrode is held at the same potential as the collar to prevent interference with the current pattern. The current required for maintaining the ring at the required potential is then measured and related to the resistivity of the formation. Because the ring electrode is narrow (~1.5 in), the result is a measurement with a 2-in vertical resolution.

### Button Resistivity Measurements ( $R_{\text{BUTTONS}}$ )

Button electrodes function the same way as the ring electrode. Each button is electrically isolated from the body of the collar but is maintained at the same potential to avoid interference with the current field. The amount of current required to maintain the button at the same potential is related to the resistivity of the mud and formation. The 1.5-in-diameter buttons can acquire azimuthal measurements within 56 sectors to produce a borehole image.

## RAB Programming

For quality control reasons, the minimum data density is one sample per 6-in interval; hence, a balance between rate of penetration (ROP) and LWD sampling rate must be determined. This relationship depends on the recording rate, the number of data channels to record, and the memory capacity of the LWD tool. The relationship between ROP and sample rate is as follows:

$$\text{ROP (ft/hr)} = 1800 / \text{sample rate} \cdot (\text{s}).$$

This equation defines the fastest ROP allowed at a given sample rate before the 1 sample per 6-in data density standard is breached. For Leg

193, the expected maximum ROP was 27 m/hr. Using this information the sample rate decided on was 20 s. The RAB was then programmed to record the following:

1. Average gamma ray (GR),
2. Average button resistivities for deep ( $R_{BD}$ ), medium ( $R_{BM}$ ), and shallow ( $R_{BS}$ ) buttons,
3. Ring resistivity ( $R_{Ring}$ ),
4. Bit resistivity ( $R_{Bit}$ ),
5. Deep button borehole imaging (BDIM),
6. Medium button borehole imaging (BMIM), and
7. Shallow button borehole imaging (BSIM).

Under this configuration the RAB has enough memory to record 71 hr of data, which was sufficient time to complete the Leg 193 LWD operations. The abbreviations are used in the LDEO-BRG log data files (see “[Related Leg Data](#)”).

### **Surface Sensors**

A series of surface sensors were used during the Leg 193 LWD operations for depth calculations and heave corrections. They are described below.

#### **Depth Encoding Sensors**

The standard LWD recording mode configuration requires only a function of depth tracking. On a floating rig, this requires the ability to measure the movement of the following:

1. Heave of the vessel by the action of waves/swells and tides,
2. Position of the traveling block in the derrick, and
3. Action of the motion compensator.

In an ideal situation, the heave and the motion compensator sensors will cancel each other out in that they will be equal and opposite actions. For example, a wave will cause the vessel to rise with respect to the seafloor, but to counteract this the motion compensator will work to keep the bit on bottom.

#### **Tensiometer Encoder**

On riser vessels, guideline cables run from the moonpool area down to the blowout prevention system (BOP) on the seafloor. Each guideline is assembled on a system of pulleys, which are mounted on a compensating piston. As waves/swells (short term) and tide (long term) are acting on the vessel, the piston is constantly working to maintain a constant tension in the guideline cable by either retracting or extending. By attaching a sensor, which is able to measure the relative position of the piston, data on the vessel’s vertical movement with respect to the seafloor can be determined. This sensor is termed the guideline tensionometer encoder (GTE).

On the *JOIDES Resolution*, the situation is complicated by the absence of a riser and a BOP system, hence no guidelines are available to be able to measure the vessel’s heave. To substitute for this the LDEO BRG has developed a wireline heave compensator (WHC). The WHC is used dur-

ing wireline logging operations by passing the wireline through a sheave on the compensator. This sheave is on a compensating piston that retracts to draw in the wireline cable during the vessel's downward movement and extends to pay out wireline cable during the vessel's upward movement. The vessel's movement is detected by accelerometers and a computer that activates the action of the compensating piston processes this information. A GTE sensor was mounted on the WHC in an attempt to integrate this information into the surface depth tracking system, and this sensor was also used to measure heave during wireline logging operations.

### **Motion Compensator and Drawworks Encoders**

The length of the drill string (combined lengths of the BHA and the drill pipe) to the top drive and the position of the top drive in the derrick is what is used to determine the exact depth of the drill bit. On a floating rig, the system is as follows:

1. Drill line is spooled on the drawworks. From the drawworks, the drill line extends to the crown blocks, which are located at the very top of the derrick, and then down to the traveling blocks. The drill line is passed several times (usually 6 or 8 times) between the traveling blocks and the crown blocks and then fastened to a fixed point called the dead-man anchor. From the driller's console, the driller controls the operation of the drawworks, which, via the pulley system described above, controls the position of the traveling blocks in the derrick.
2. On a fixed rig (i.e., a rig situated either on a platform or on land) the top drive will be suspended from the traveling blocks; however, on a floating rig the motion compensator is suspended from the traveling blocks. The top drive is then attached to the motion compensator. The motion compensator uses pistons in a compensator that are held to a precharge; thus, they are able to provide a buffer against the waves and swell. As the vessel rises, the compensator extends the pistons under the pressure of the precharge to keep the bit on bottom; whereas, when the vessel drops, the pistons retract and diffuse any extra weight from being stacked on the bit.
3. The drill string is housed directly in the top drive; therefore, it is the movement of the top drive that needs to be measured to provide depth tracking. The top drive also provides the rotation to the drill string and is where the drilling fluid (mud) enters the drill pipe.

To measure the movement of the traveling blocks a drawworks encoder (DWE) is usually mounted on the shaft of the drawworks. One revolution of the drawworks will pay out a certain amount of drill line, and in turn move the traveling blocks a certain distance. Calibration of the movement of the traveling block to the revolution of the drawworks needs to be performed.

A motion compensator encoder (MCE) operates in exactly the same way as the GTE in that a length of thin wire on a spring-loaded retrieval system is attached to the top drive while the retrieval system and encoder section are attached to a fixed point above the compensating pistons. As the pistons are either extending or retracting to compensate for

the heave of the ship, the encoder measures the amount of wire being paid out or being fed back into the retrieval system.

The combination of DWE and MCE sensors that provide LWD depth tracking capabilities can be incorporated into a single sensor that operates off a geolograph line. The geolograph line is a cable that is attached directly to the top drive. A cable retrieval system and encoding sensor is attached to a fixed point on or near the rig floor. The geolograph line then travels up and down the derrick with the top drive while the encoder measures the amount of line being paid out or retrieved. The geolograph system requires no calibration.

All the systems described above effectively work to provide similar information and are applicable for use on the *JOIDES Resolution*. Although these systems were tested during Leg 193, only the geolograph and GTE systems were used during LWD operations.

### **Hookload Sensor**

The hookload sensor is used to measure the weight of the load on the drill string to detect whether the drill string is “in slips” or “out of slips.” When the drill string is in slips, motion from the blocks or motion compensator will not have any effect on the depth of the bit (i.e., it will remain stationary), and when the drill string is out of slips, the reverse is true. The difference in hookload weight between in slips and out of slips is quite distinguishable. The heave of the ship (measured by the GTE sensor) will still continue to affect the bit depth whether the drill string is in slips or out of slips.

### **Standpipe Pressure Sensor**

The standpipe pressure sensor is used to measure the pressure acting on the drilling fluid in the standpipe. Although standpipe pressure is not a necessary measurement, it can be useful for the logging engineer. Also, with no mud logging service company on the *JOIDES Resolution*, the standpipe pressure sensor can provide pumping time information for the bit run.

### **Software Filtering of Heave**

Software filtering provides a smoothing of the time-depth file by taking data immediately before and after a given point and applying a weighted averaging algorithm to the depth file. The depth filtering technique has a marked effect on improving the quality of the logs and was applied to the Leg 193 RAB data.

## REFERENCES

- Blum, P., 1997. Physical properties handbook: a guide to the shipboard measurement of physical properties of deep-sea cores. *ODP Tech. Note*, 26 [Online]. Available from World Wide Web: <<http://www-odp.tamu.edu/publications/tnotes/tn26/INDEX.HTM>>. [Cited 2000-11-07]
- Bonner, S., Burgess, T., Clark, B., et al., 1993. Measurements at the bit: a new generation of MWD tools. *Oilfield Rev.*, Apr./Jul., 44–54.
- Davis, E.E., Mottl, M.J., Fisher, A.T., et al., 1992. *Proc. ODP, Init. Repts.*, 139: College Station, TX (Ocean Drilling Program).
- Deer, W.A., Howie, R.A., and Zussman, J., 1992. *An Introduction to the Rock-Forming Minerals* (2nd ed.): London (Longman).
- Duffield, W.A., and Dalrymple, G.B., 1990. The Taylor Creek Rhyolite of New Mexico: a rapidly emplaced field of lava domes and flows. *Bull. Volcanol.*, 52:475–487.
- Ellis, D.V., 1987. *Well Logging for Earth Scientists*: New York (Elsevier).
- Fink, J.H., and Manley, C.R., 1987. Origin of pumiceous and glassy textures in rhyolitic flows and domes. *Geol. Soc. Am. Spec. Pap.*, 212:77–88.
- Fouquet, Y., Zierenberg, R.A., Miller, D.J., et al., 1998. *Proc. ODP, Init. Repts.*, 169: College Station, TX (Ocean Drilling Program).
- Gieskes, J.M., Gamo, T., and Brumsack, H., 1991. Chemical methods for interstitial water analysis aboard *JOIDES Resolution*. *ODP Tech. Note*, 15.
- GRC, 1994a. *Multi-Sensor Memory Module Operation Manual*, Document #006-0112-00: Tulsa, OK (Geophysical Research Corporation).
- , 1994b. *University of Miami UHT-MSM Operations Manual*, Document #006-0122-00: Tulsa, OK (Geophysical Research Corporation).
- , 1996. *MSM/MIAMI Operation Software (Revision 0) User's Guide*, Document #006-0128-00: Tulsa, OK (Geophysical Research Corporation).
- Holcombe, R.J., 1996. *Georient 4.2: Stereographic projections and rose diagram plots. Computer programme for plotting structural data*. Dept. Earth Sci., Univ. Queensland.
- Hoppie, B.W., Blum, P., and the Shipboard Scientific Party, 1994. Natural gamma-ray measurements on ODP cores: introduction to procedures with examples from Leg 150. In Mountain, G.S., Miller, K.G., Blum, P., et al., *Proc. ODP, Init. Repts.*, 150: College Station, TX (Ocean Drilling Program), 51–59.
- Humphris, S.E., Herzig, P.M., Miller, D.J., et al., 1996. *Proc. ODP, Init. Repts.*, 158: College Station, TX (Ocean Drilling Program).
- Kano, K., Takeushi, K., Yamamoto, T., and Hoshizumi, H., 1991. Subaqueous rhyolite block lavas in the Miocene Ushikiri Formation, Shimane Peninsula, SW Japan. *J. Volcanol. Geotherm. Res.*, 46:241–253.
- Kirschvink, J.L., 1980. The least-squares line and plane and the analysis of palaeomagnetic data. *Geophys. J. R. Astron. Soc.*, 62:699–718.
- LeMaitre, R., 1976. A new approach to the classification of igneous rocks using the basalt-andesite-dacite-rhyolite suite as an example. *Contrib. Mineral. Petrol.*, 56:191–203.
- MacKenzie, W.S., Donaldson, C.H., and Guilford, C., 1982. *Atlas of Igneous Rocks and their Textures*: Harlow, England (Longman).
- McPhie, J., Doyle, M., and Allen, R., 1993. *Volcanic Textures—A Guide to the Interpretation of Textures in Volcanic Rocks*: Univ. Tasmania, Cent. Ore Deposit Explor. Stud., Hobart, Australia.
- Murray, R.W., Miller, D.J., and Kryc, K.A., 2000. Analysis of major and trace elements in rocks, sediments, and interstitial waters by inductively coupled plasma–atomic emission spectrometry (ICP-AES). *ODP Tech. Note*, 29 [Online]. Available from World Wide Web: <<http://www-odp.tamu.edu/publications/tnotes/tn29/INDEX.HTM>>. [Cited 2000-11-07]

- Plank, T., Ludden, J.N., Escutia, C., et al., 2000. *Proc. ODP, Init. Repts.*, 185 [CD-ROM]. Available from: Ocean Drilling Program, Texas A&M University, College Station TX 77845-9547, USA.
- Rider, M., 1996. *The Geological Interpretation of Well Logs* (2nd ed.): Caithness (Whittles Publishing).
- Sass, J.H., Kennelly, J.P., Jr., Smith, E.P., and Wendt, W.E., 1984. Laboratory line-source methods for the measurement of thermal conductivity of rocks near room temperature. *U.S. Geol. Surv. Tech. Rep.*, 84–91.
- Schlumberger, 1989. *Log Interpretation Principles/Applications*: Houston (Schlumberger Educ. Services), SMP-7017.
- , 1995. *DSI—Dipole Sonic Imager*: Houston (Schlumberger Wireline and Testing), SMP-5128.
- Serra, O., 1984. *Fundamentals of Well-Log Interpretation* (Vol. 1): *The Acquisition of Logging Data*: Dev. Pet. Sci., 15A.
- Shipboard Scientific Party, 1991. Explanatory notes. In Davies, P.J., McKenzie, J.A., Palmer-Julson, A., et al., *Proc. ODP, Init. Repts.*, 133 (Pt. 1): College Station, TX (Ocean Drilling Program), 31–58.
- , 1997. Explanatory notes. In Eberli, G.P., Swart, P.K., Malone, M.J., et al., *Proc. ODP, Init. Repts.*, 166: College Station, TX (Ocean Drilling Program), 43–65.
- , 1998. Explanatory notes. In Fouquet, Y., Zierenberg, R.A., Miller, D.J., et al., *Proc. ODP, Init. Repts.*, 169: College Station, TX (Ocean Drilling Program), 17–32.
- , 2001. Explanatory notes. In Christie, D.M., Pedersen, R.-B., Miller, D.J., et al., *Proc. ODP, Init. Repts.*, 187, 1–42 [CD-ROM]. Available from: Ocean Drilling Program, Texas A&M University, College Station, TX 77845-9547, USA.
- , 2001. *Proc. ODP, Init. Repts.*, 191: College Station, TX (Ocean Drilling Program).
- Smith, D.C., Spivack, A.J., Fisk, M.R., Haveman, S.A., Staudigel, H., and ODP Leg 185 Shipboard Scientific Party, 2000. Methods for quantifying potential microbial contamination during deep ocean coring. *ODP Tech. Note*, 28 [Online]. Available from the World Wide Web: <<http://www-odp.tamu.edu/publications/tnotes/tn28/INDEX.HTM>>. [Cited 2000-11-07]
- Vacquier, V., 1985. The measurement of thermal conductivity of solids with a transient linear heat source on the plane surface of a poorly conducting body. *Earth Planet. Sci. Lett.*, 74:275–279.
- Waters, J.C., Binns, R.A., and Naka, J., 1996. Morphology of submarine felsic volcanic rocks on Pual Ridge, eastern Manus Basin, Papua New Guinea. *Eos*, WPGM Supplement, 77:W120.
- Yamagishi, H., 1987. Studies on the Neogene subaqueous lavas and hyaloclastites in southwest Hokkaido. *Rept. Geol. Surv. Hokkaido*, 59:55–117.
- Zijderveld, J.D.A., 1967. A. C. demagnetization of rocks: analysis of results. In Collinson, D.W., Creer, K.N., and Runcorn, S.K. (Eds.), *Methods in Paleomagnetism*: Amsterdam (Elsevier), 254–286.

Figure F1. Schematic examples of numbered core sections.

ODP LEG 193  
SITE 1188

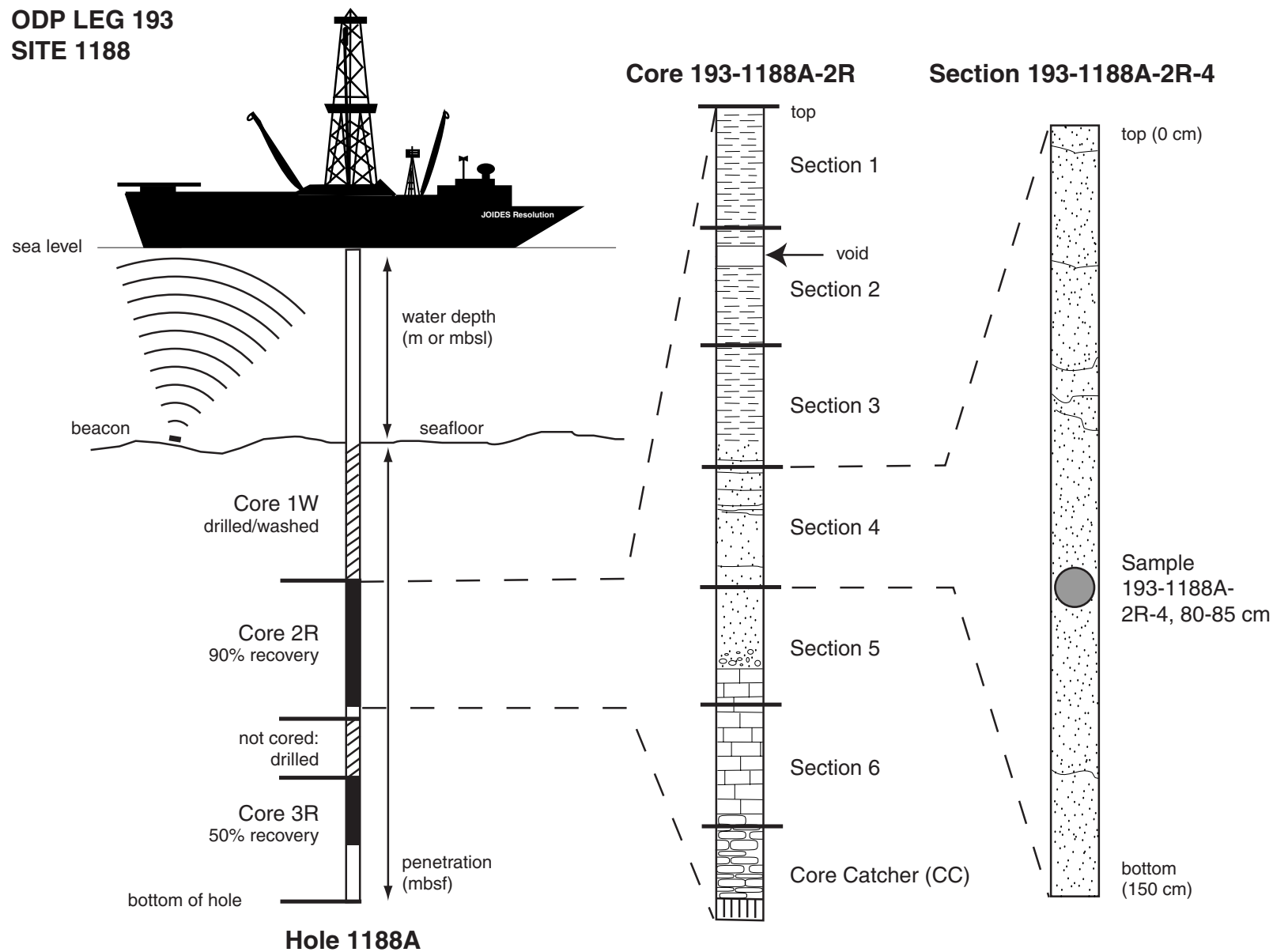


Figure F2. A. Fragmented but essentially intact ADCB core (Core 193-1188F-2Z). (Continued on next page.)

**A**



Figure F2 (continued). B. Fragments of rubble as extracted from the ADCB core barrel. In some cases, pieces that could be fit together indicated a coherent core had been cut that fell apart upon extraction from the core barrel. In many other cases, the core is so fragmented that it is not possible to determine if the rubble is a drilling-induced artifact or a result of postcoring disintegration (Core 193-1188F-41Z).

**B**



Figure F3. Calibration curve used during Leg 193 to estimate the glass compositions (bulk silica content, recalculated volatile free; based on dredged samples from PACMANUS cruises, 1991–1997; R.A. Binns, pers. comm., 2000). As much as 20% of microlites or phenocrysts do not seriously affect the use of the diagram, although some judgement might be required at the dacite-rhyodacite boundary (70% SiO<sub>2</sub>).

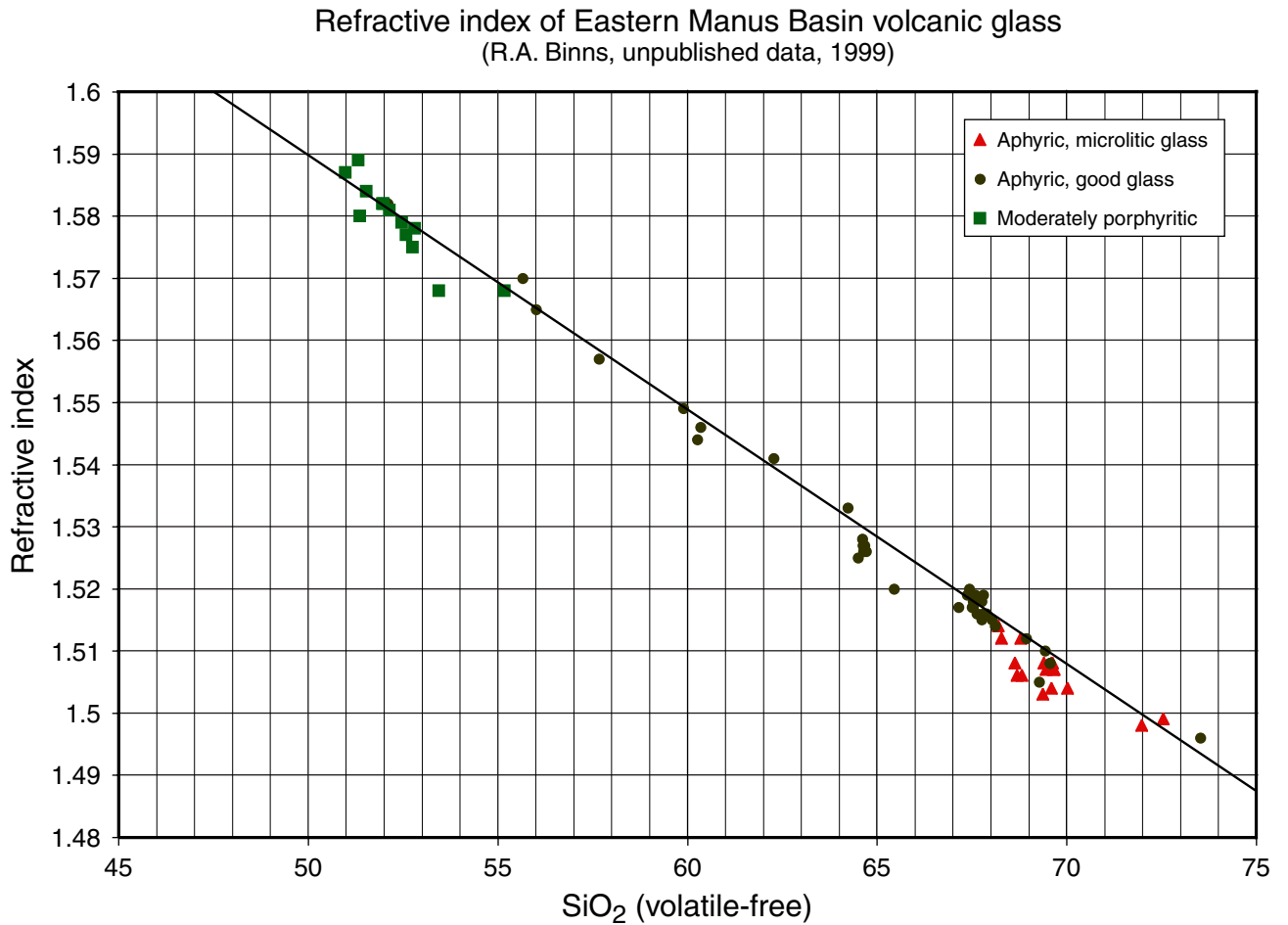
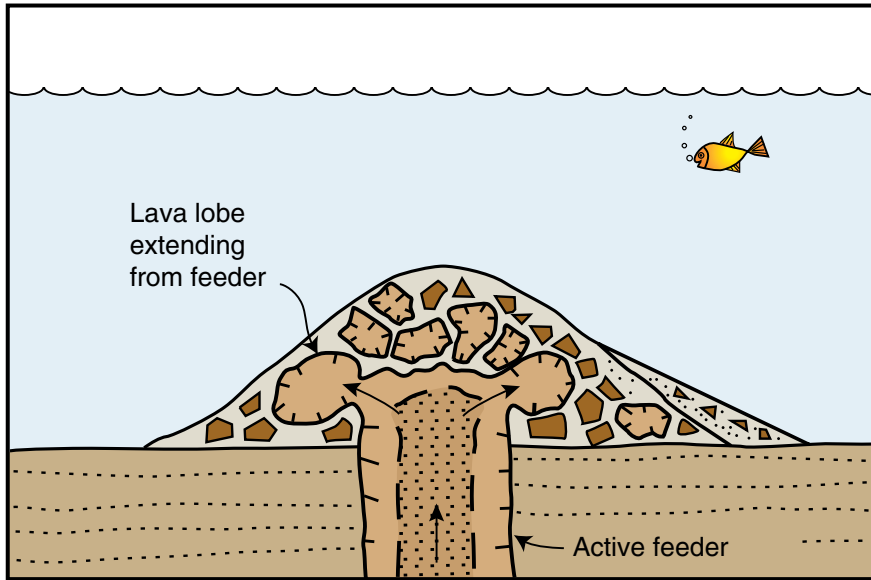


Figure F4. Conceptual sketch of a subaqueous, in situ, and resedimented hyaloclastite and feeder dike. A. Lava emerging from the feeder dike advances a short distance before being quenched. B. The growing hyaloclastite pile is intruded by its feeder dike. Unstable in situ hyaloclastite is resedimented downslope (from McPhie et al., 1993; modified from Yamagishi, 1987).

A



B

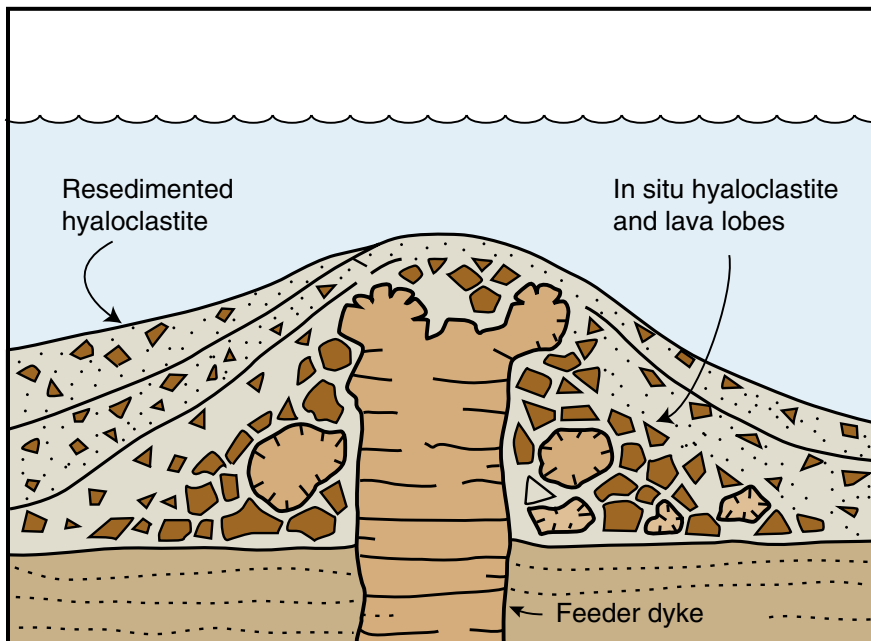
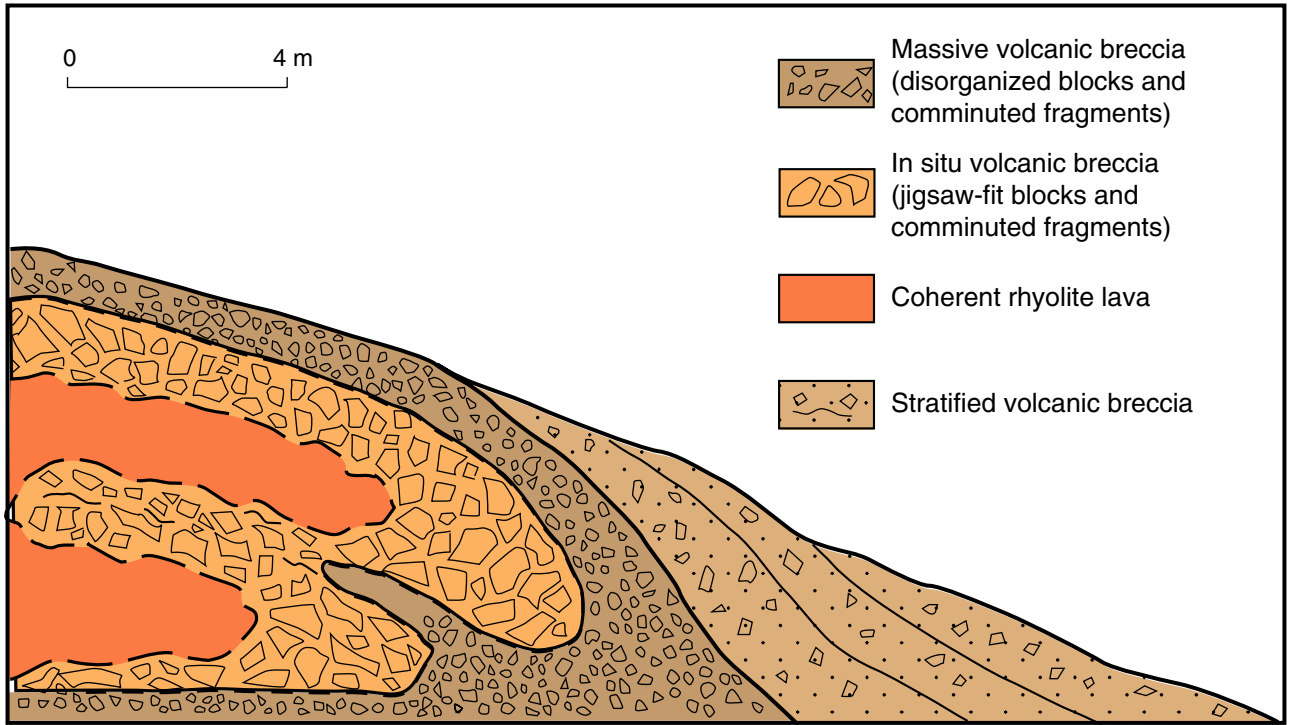
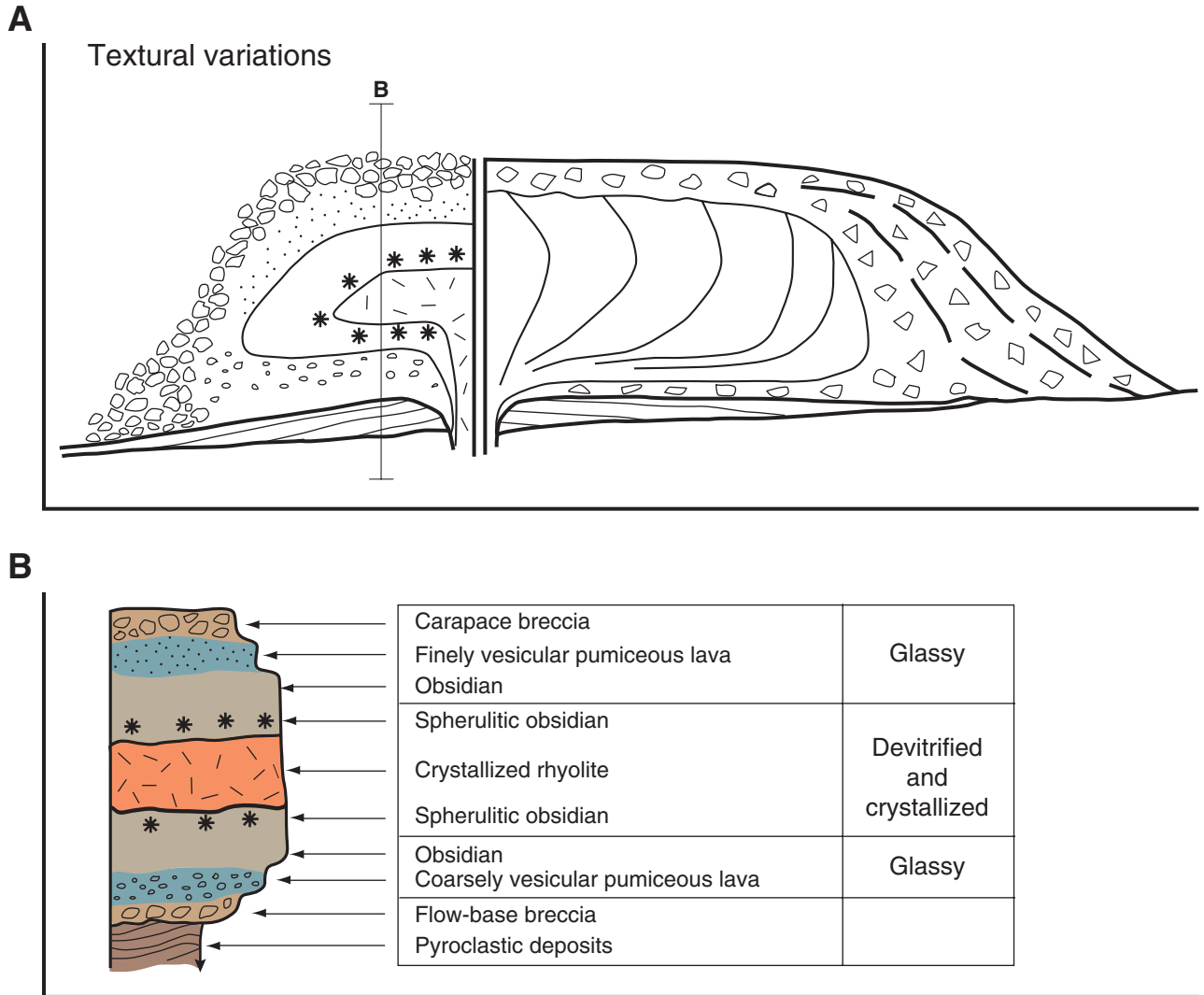


Figure F5. Schematic volcanic facies associated with subaqueous emplacement of siliceous lava (Miocene, Ushikiri Formation, Japan) (from McPhie et al., 1993; modified from Kano et al., 1991).



**Figure F6.** A. Schematic cross section through a subaerial silicic lava flow. The left side shows the internal textural variations arising from vesiculation, devitrification, and flow fragmentation. The right side shows the orientations of internal flow foliations and crude layering in flow margin talus breccia. B. The vertical section through the flow at the position is indicated in (A), showing the major textural zones (from McPhie et al., 1993; modified from Fink and Manley, 1987, and Duffield and Dalrymple, 1990).



**Figure F7.** Key to the graphical patterns used to summarize lithologies, alteration styles, and mineralization styles in the visual core descriptions.

**Symbols used in Leg 193 Visual Core Descriptions**

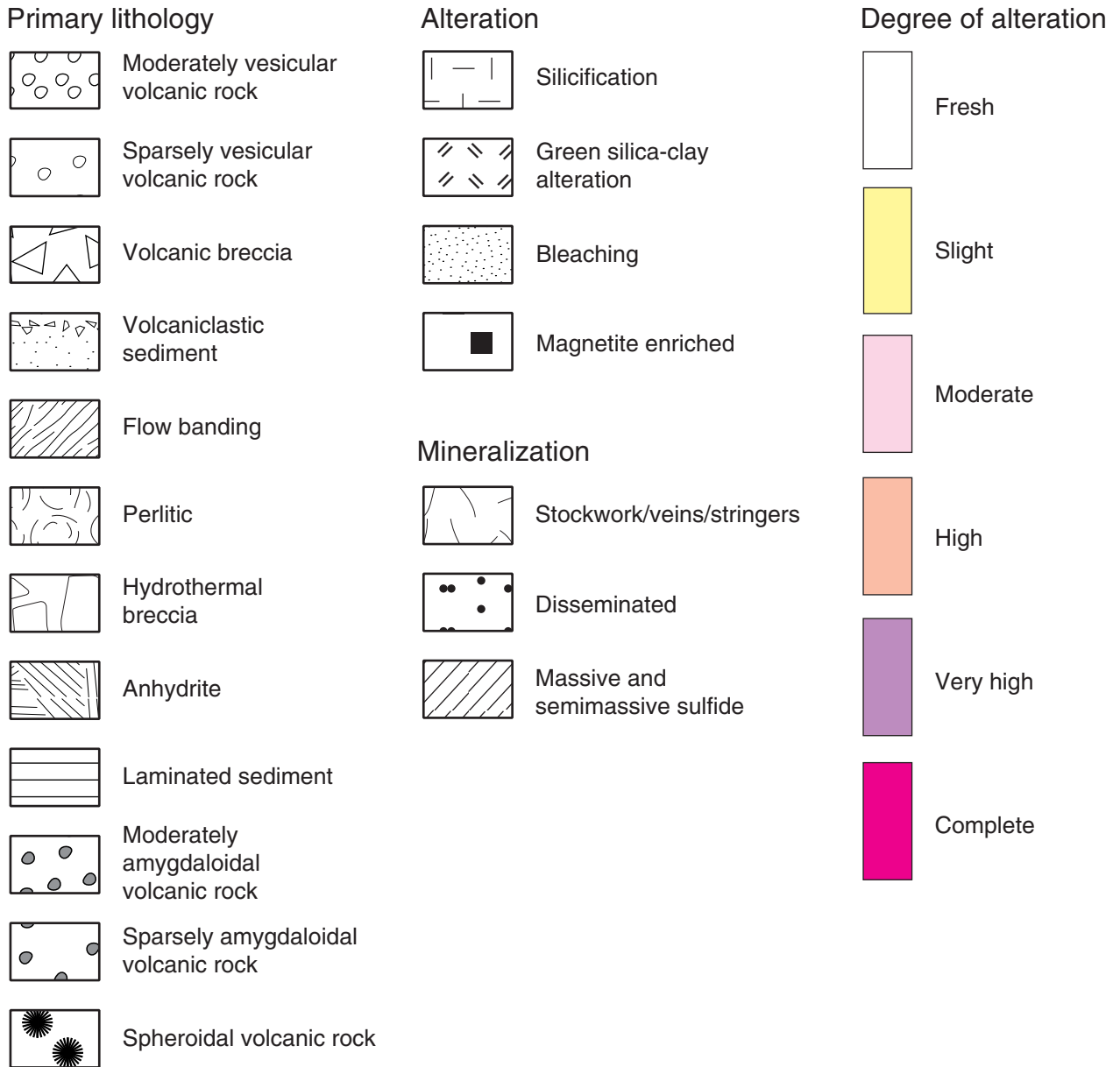






**Figure F10.** Conventions used during Leg 193 to measure the orientation of structures in cores. Most orientations were constructed from two apparent dips measured as lineations on the archive face and on one side of the archive half of the core (the side face), which was assumed to be at 90° to the archive face. For the purpose of plotting the data and also recording the data, the plane perpendicular to the core axis was regarded as the horizontal plane of a stereographic net with relative north being the bottom of the core liner of the archive half. The right side was chosen to be relative east, and the left side was chosen to be relative west.

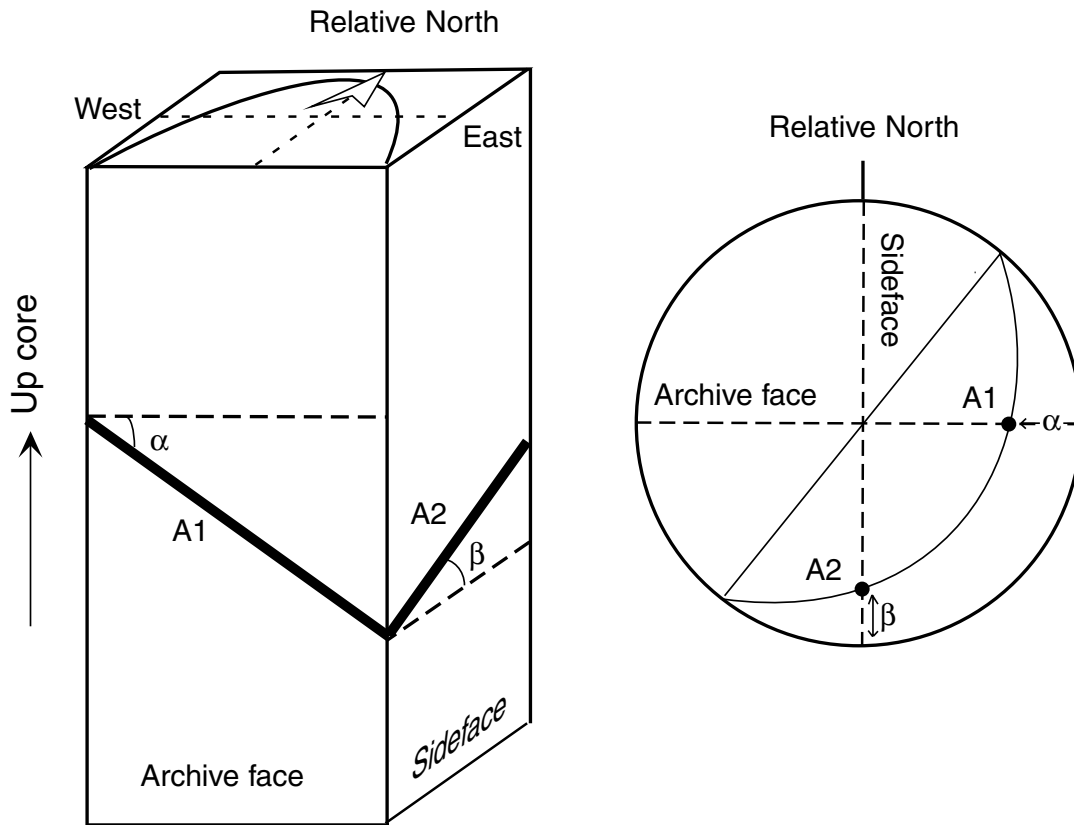


Figure F11. Example of an on-board structural geology description form.

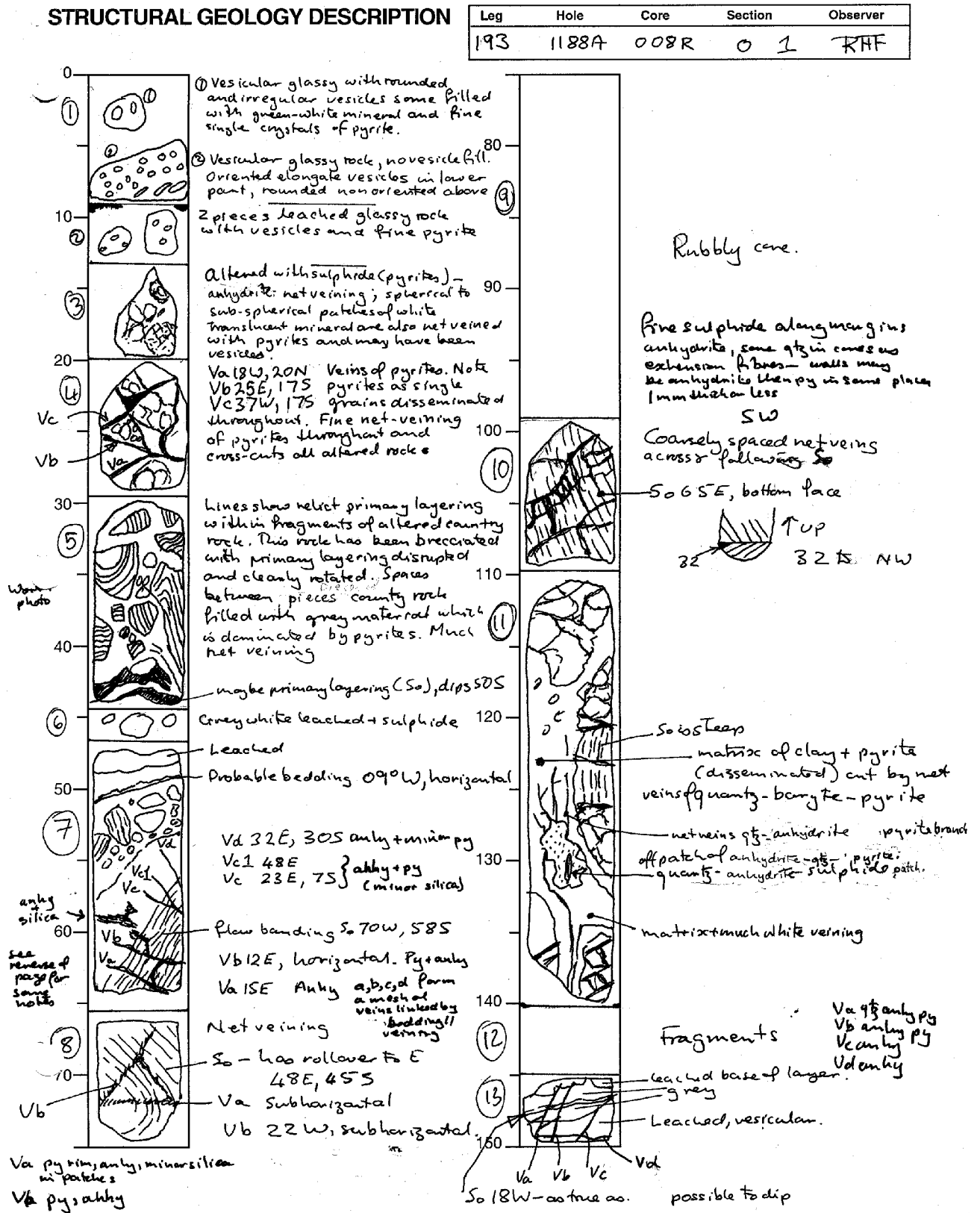


Figure F12. Relationship between vesicles and flowbanding in a volcanic rock exposed to simple shear and pure shear deformation, respectively.

Undeformed volcanic rock  
with flowbanding and vesicle

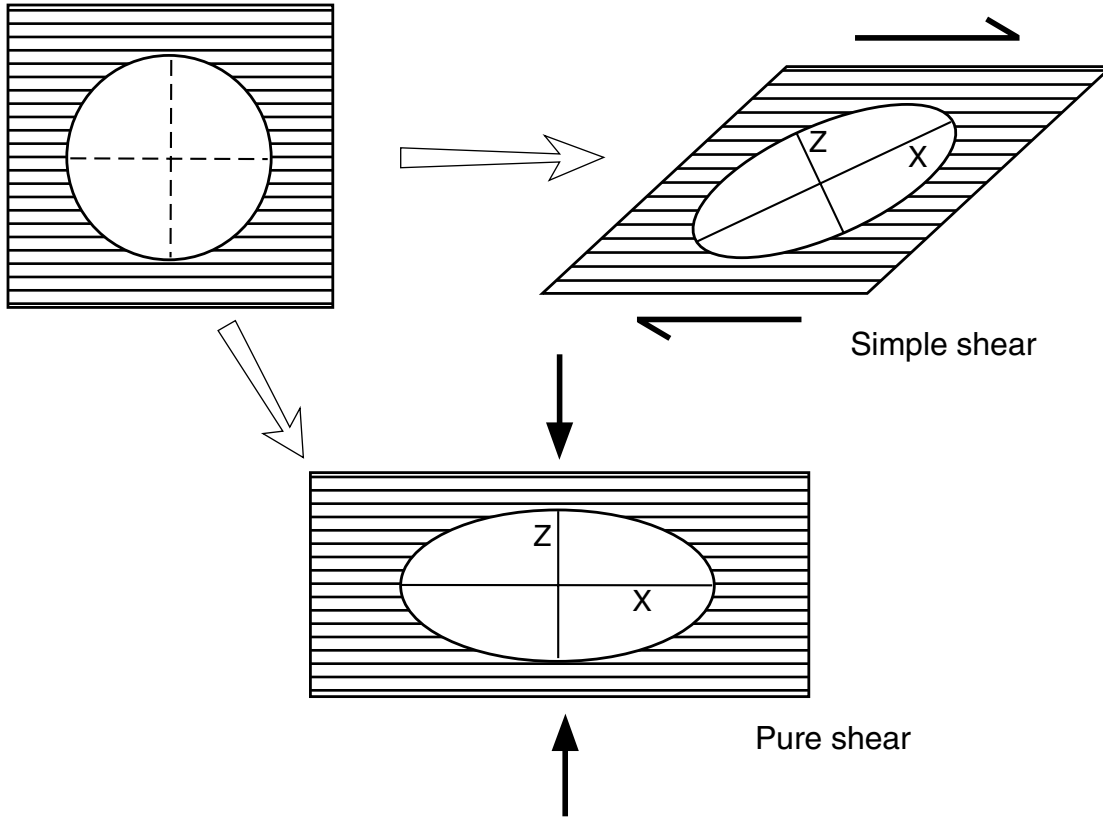


Figure F13. Orientation convention for ODP cores and discrete samples.

ODP magnetic direction convention

A



Minicore

B

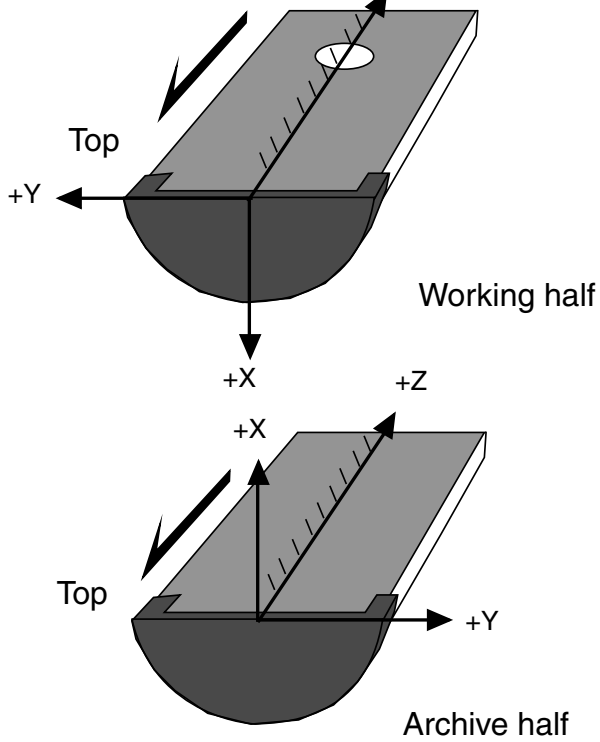
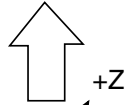


**Figure F14.** Steps for assembling the core barrel temperature tool: (A) assembled the electronics with the encased battery and vespel plug next to the dewar; (B) the assembled dewar with electronics inside; (C) insert the tool inside the pressure case (notice the yellow fishing neck) (the latching tool attaches to this piece when retrieving the CBTT and core barrel assembly); and (D) the tool is attached to the core barrel.



Figure F15. Core barrel temperature tool tests performed at the Lamont-Doherty Earth Observatory showing the effectiveness of the insulating properties of the dewar system with and without glycerin.

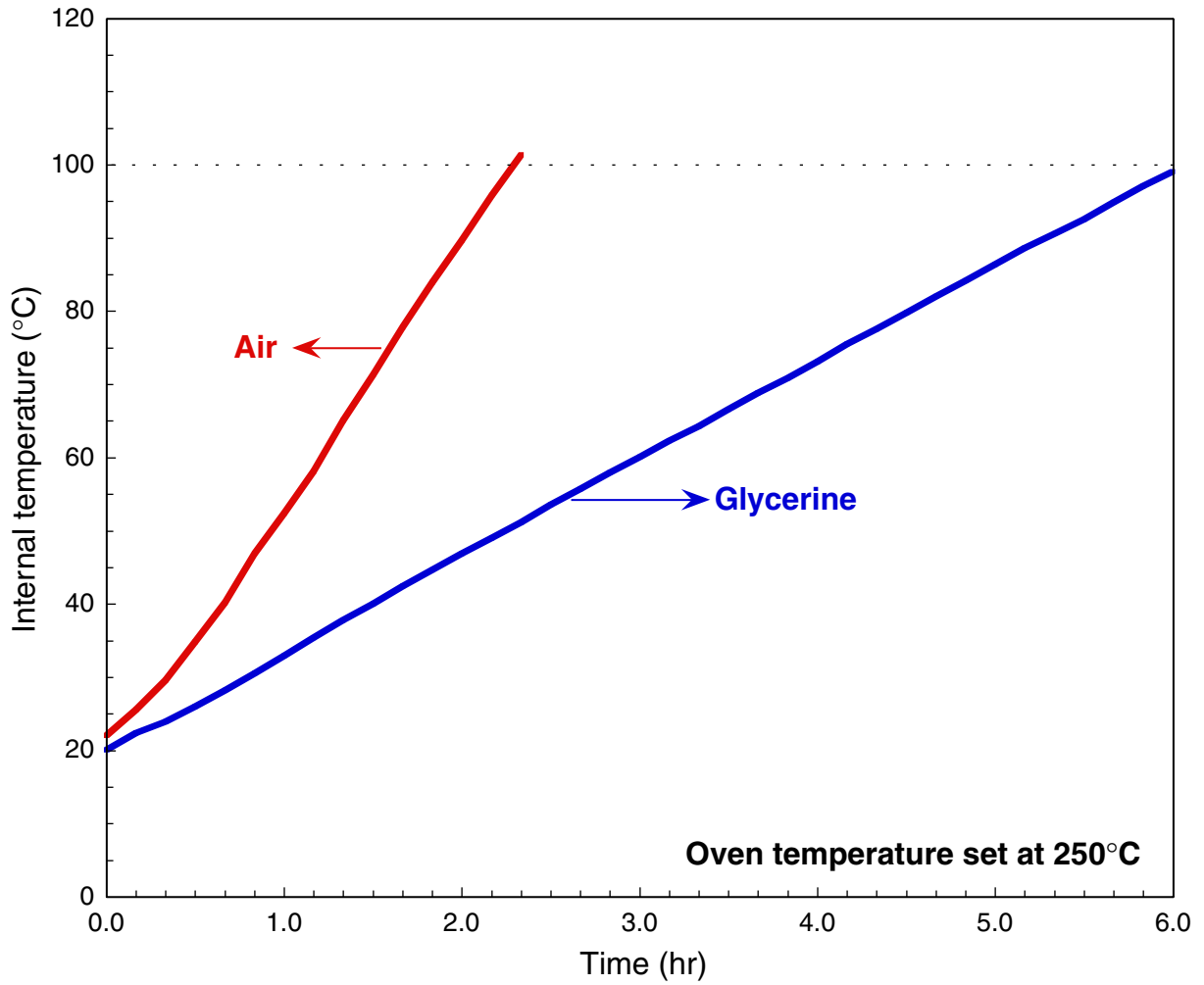
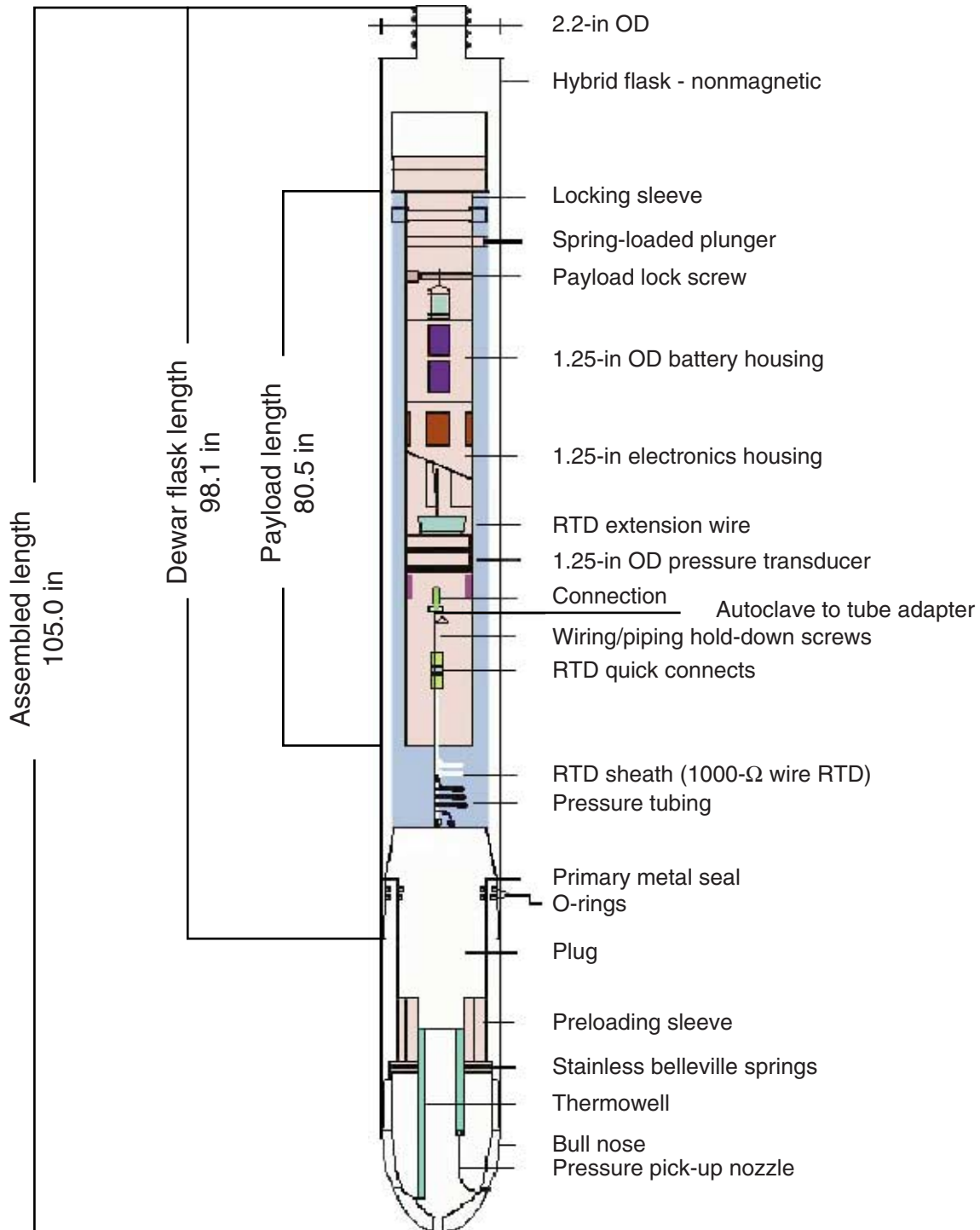


Figure F16. Schematic diagram showing the major components of the ultra high temperature multisensor memory (UHT-MSM) tool (not to scale) (from Shipboard Scientific Party, 1998). OD = outer diameter. RTD = resistance temperature detector.



**Figure F17.** Schematic diagram of the triple combination and Formation Microscanner (FMS)/sonic tool strings. HTCG = high-temperature/pressure telemetry gamma-ray cartridge. HNGS = hostile-environment natural gamma-ray sonde. APS = accelerator porosity sonde. HLDS = hostile-environment lithodensity sonde. DSI = dipole shear imager. NGT = natural gamma-ray tool. GDIT = general purpose inclinometer tool.

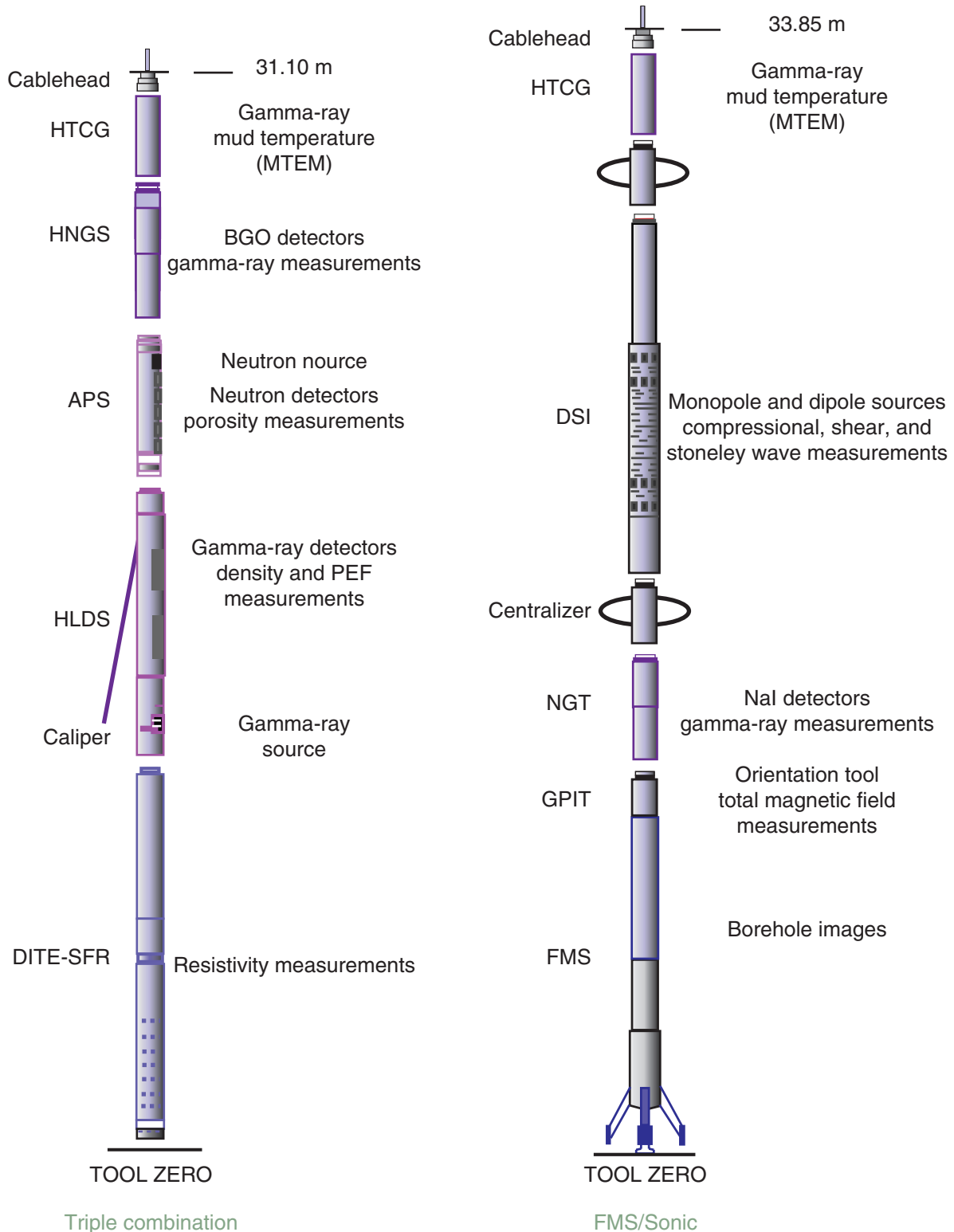


Figure F18. Calibration performed for the MTEM sensor at the Schlumberger Offshore Division facilities in Houston. **A.** Six-point measurements made with a calibrated thermocouple and the MTEM sensor. **B.** Correlation between measurements made with the thermocouple and MTEM sensors.  $T_{tc}$  = temperature reading from thermocouple.  $T_{mtem}$  = temperature reading from MTEM.

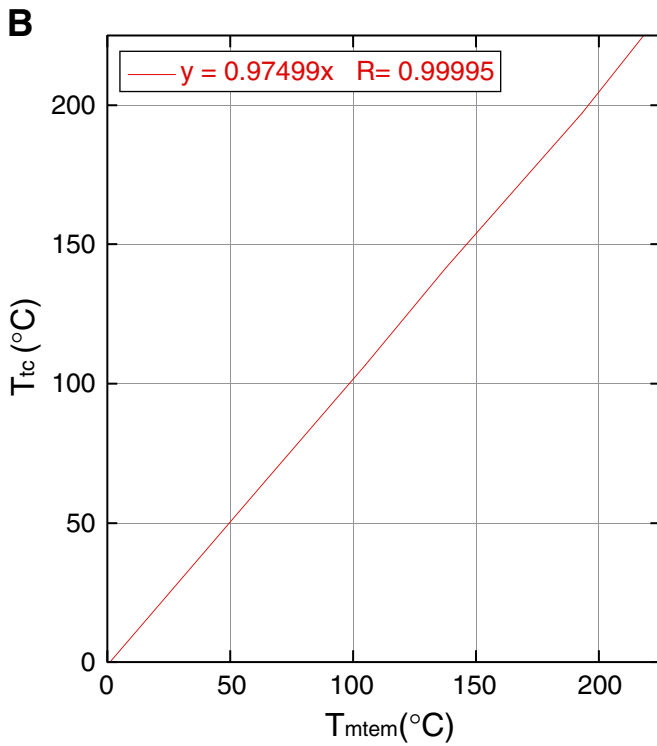
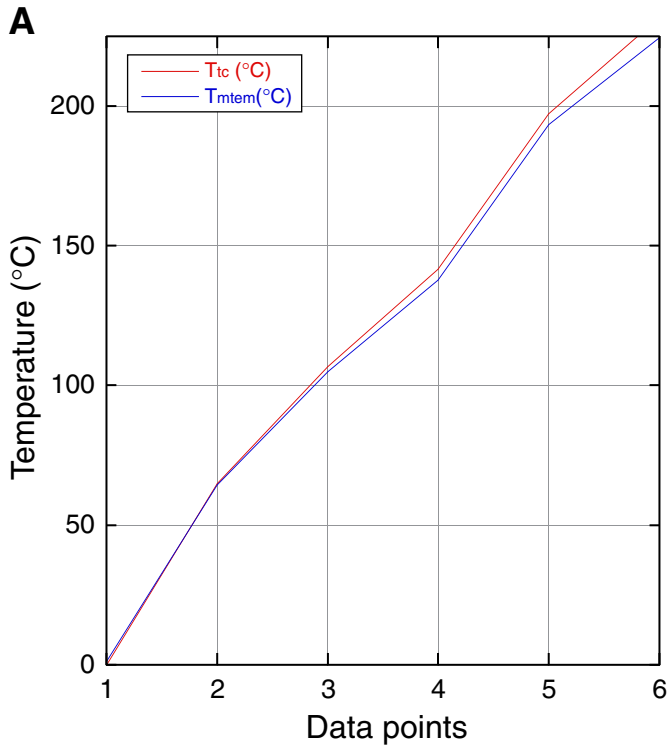
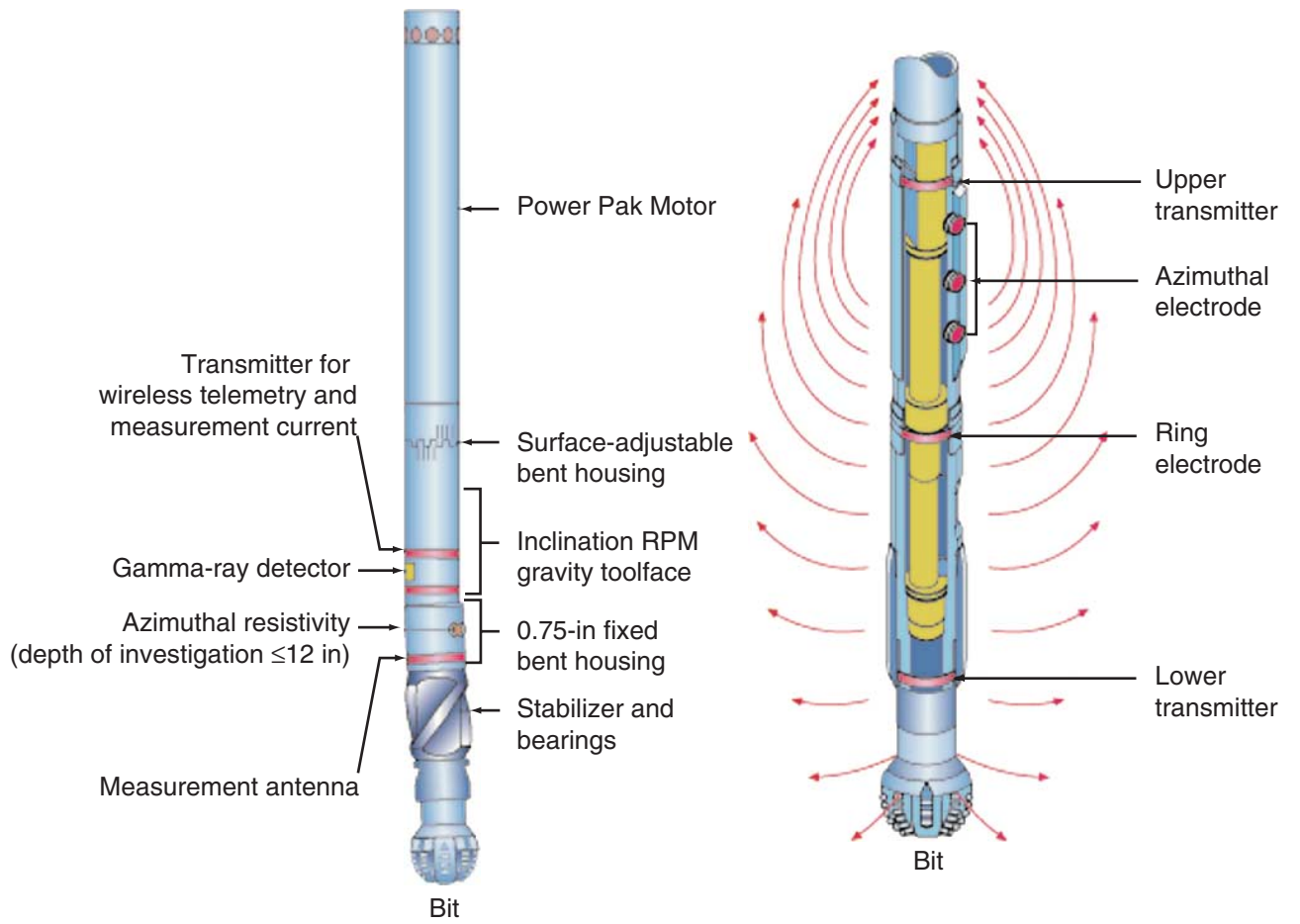
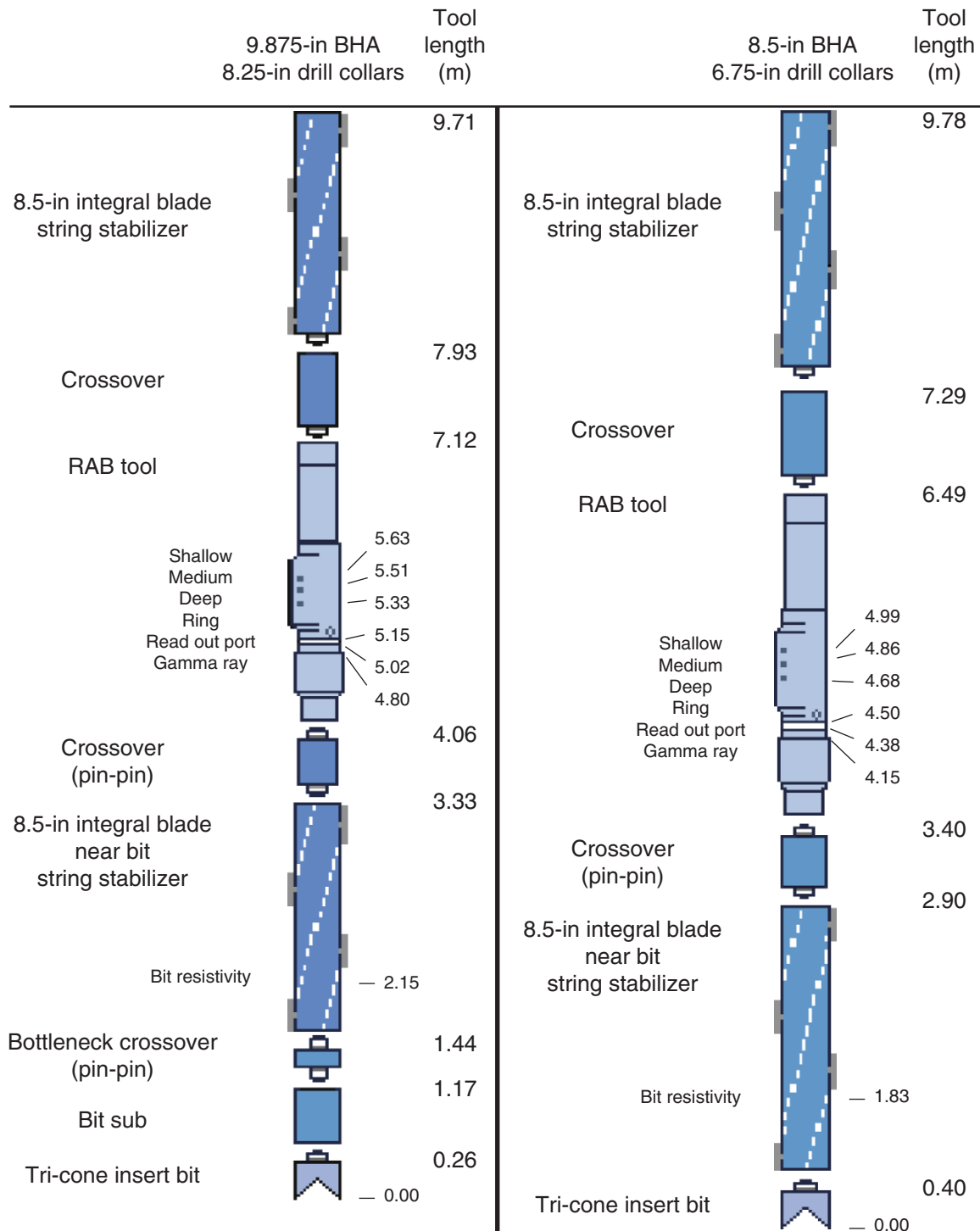


Figure F19. Schematic diagram of the resistivity-at-the-bit (RAB) tool (modified from Bonner et al., 1993).



**Figure F20.** Schematic diagram of the resistivity-at-the-bit (RAB) tool and the two different types of bottom-hole assemblies (BHA) that were available during Leg 193.



**Table T1.** Abbreviations for technical terms, Leg 193.  
(Continued on next page.)

Abbreviation	Definition
ADCB	advanced diamond core barrel
AF	alternating field
AFM	atomic force microscopic
AHC	active heave compensator
AMS	anisotropy of magnetic susceptibility
AMST	archive MST
APC	advanced hydraulic piston corer
API	American Petroleum Institute (unit)
APS	accelerator porosity sonde
ARM	anhysteretic remanent magnetization
ASC	Analytical Services Company
ATP	adenosine triphosphate
BGO	bismuth germanate
BHA	bottom-hole assembly
BOP	blowout prevention system
BRG	Borehole Research Group
CBTT	core barrel temperature tool
DAPI	4,6-diamindino-2-phenylindole
DC-SQUID	direct current superconducting quantum interference device
DES	dual elevator stool
DHML	downhole measurements laboratory
DIT	dual induction resistivity
DP	dynamic positioning
DSA	drill string accelerometer
DSI	dipole shear imager
DWE	drawworks encoder
FFF	free-fall funnel
FFSW	formaldehyde in artificial seawater
FMS	Formation MicroScanner
FTIR	fluorier transmission infrared spectroscopic
GFI	ground fault interrupt
GPS	Global Positioning System
GRA	gamma-ray attenuation
GSC	green silica-clay
GTE	guideline tensionometer encoder
HEPES	N-2-hydroxyethylpiperazine-N-2- ethanesulfonic acid
HLDS	hostile-environment lithodensity sonde
HNGS	hostile-environment natural gamma-ray sonde
HRRS	hard-rock reentry system
HTGC	high-temperature/pressure telemetry gamma-ray cartridge
HTT	high-temperature tool
IC	ion chromatography
ICP-AES	inductively coupled plasma-atomic emission spectroscopy
IRM	isothermal remanent magnetization
IUGS	International Union of Geological Sciences
<i>k</i>	whole-core magnetic susceptibility
<i>k<sub>ij</sub></i>	susceptibility tensor
kips	1000 lb
LDEO	Lamont-Doherty Earth Observatory
LOI	loss on ignition
LWD	logging while drilling
MBR	mechanical bit release
mbrf	meters below rig floor
mbsf	meters below seafloor
MCE	motion compensator encoder
MORB	mid-ocean-ridge basalt
MSM	magnetic susceptibility meter
MST	multisensor track
MTEM	real-time cable head temperature capabilities
NAA	neutron activation analysis
NCS	nitrogen, carbon, sulfur
NGR	natural gamma radiation
NGT	natural gamma-ray tool

**Table T1 (continued).**

Abbreviation	Definition
ODP	Ocean Drilling Program
PACMANUS	Papua New Guinea-Australia-Canada-Manus
PBS	phosphate buffer saline
PDR	precision depth recorder
PFT	perfluorocarbon tracer
PHC	passive heave compensator
PIMA	portable infrared mineral analyzer
PNG	Papua New Guinea
ppg	pounds per gallon
<i>P</i> -wave	compressional wave
PWL	compressional wave logger
PWS3	contact probe system
Q	the Koengsberger ratio
RAB	resistivity at the bit
RCB	rotary core barrel
RI	refractive index
ROP	rate of penetration
RPM	revolutions per minute
RRING	focused lateral resistivity measurement
SEM	scanning electron microscopic
spm	strokes per minute
<i>S</i> -wave	shear wave
SWIR	shortwave infrared
TAMU	Texas A&M University
TCA	trichloroacetic acid
TD	total depth
TEM	transmission electron microscopic
triple combo	triple combination (tool string)
TSF	Transocean Sedco Forex
UHT-MSM	ultra high temperature multisensor memory tool
VCD	visual core description
VIT	vibration-isolated television
WHC	wireline heave compensator
WOB	weight on bit
WSTP	water-sampling temperature probe
XRD	X-ray diffraction

**Table T2.** Abbreviations used in the alteration/mineralization and vein/structure descriptions.

Term	Abbreviation	Term	Abbreviation
<b>Common colors:</b>		<b>Sulfide mineralization style:</b>	
Black	Blk	Massive	MS
White	Wht	Semimassive	SMS
Brown	Brn	Disseminated	DS
Yellow	Yel	Vein/stringer	VS
Olive	Olv	Sulfide breccia	SB
Green	Grn	Vug/vesicle fill	VF
Gray	Gr	<b>Sulfide mineralogy:</b>	
Blue	Bl	Bornite	Bn
Red	Rd	Chalcopyrite	Cp
Pink	Pk	Covellite	Cv
Tan	Tn	Enargite	En
Gold	Gd	Galena	Gn
Dark	Dk	Marcasite	Mc
Light	Lt	Pyrite	Py
<b>Grain size:</b>		Sphalerite	Sp
Very fine (<0.5 mm)	vfg	Tetrahedrite	Tt
Fine (0.5-1 mm)	fg	Tennantite	Tn
Medium (>1-2 mm)	mg	<b>Apparent vein orientation:</b>	
Coarse (>2 mm)	cg	Inclined	INC
<b>Alteration intensity:</b>		Curved	CUR
Fresh (<2%)	Fr	Horizontal	H
Slight (2%-<10%)	Sl	Vertical	V
Moderate (10%-<40%)	Md	Subhorizontal	SH
High (40%-<80%)	Hi	Subvertical	SV
Very high (80%-<95%)	VH	Stockwork	SW
Complete (95%-100%)	Cm	Irregular	IR
<b>Alteration style:</b>		<b>Other:</b>	
Pervasive	Pv	Much less than	<<
Patchy	Pa	Hairline fracture	HF
Stockwork	SW	Altered to	->
Veins	Vn	Trace (<1%)	tr
Vesicle fill	Vf	Sediment	Sed.
<b>Alteration type:</b>		Apparent	App.
Bleached	Bl	Ditto	do
Siliceous	Sil	<hr/>	
Oxidized	Ox		
Film	F		
Sulfate veins	Sv		
Green silica-clay	GSC		
Magnetite-bearing	Mt		
Mineralized	Min		
<b>Primary and alteration minerals:</b>			
Anhydrite	Anhy		
Barite	Ba		
Calcium carbonate	CO <sub>3</sub>		
Chalcedony	Chal		
Chlorite	Chl		
Clay minerals and phyllosilicates (undifferentiated)	Cl		
Epidote	Ep		
Kaolinite	Ka		
Hematite	Hem		
Iron oxyhydroxides	FeO <sub>x</sub>		
Magnetite	Mt		
Manganese oxyhydroxides	MnOx		
Native sulfur	S		
Olivine	Ol		
Plagioclase	Plag		
Pyroxene	Px		
Quartz	Qtz		
Sericite	Ser		
Silica	Si		
Smectite	Sm		
Sulfate (undifferentiated)	Sf		
Zeolite	Zeol		





**Table T5.** Textural terms and abbreviations used to describe sulfide mineralization.

	Abbreviation	Description
Styles of mineralization:		
Massive sulfide	MS	Rocks containing >75% sulfide minerals.
Semimassive sulfide	SMS	Rocks containing >25%-75% sulfide minerals, which form aggregates or intergrowths.
Disseminated sulfide	DS	Rocks containing 5%-25% disseminated sulfides.
Void fill	VF	Minerals partially or totally filling a void (vesicle, etc.).
Vein/stringer sulfide	VS	Rocks containing more than 5% sulfide in veins.
General terminology for mineral textures:		
Atoll	at	Minerals surrounded and partially replaced by another.
Banded	bnd	Precipitates showing rhythmic compositional or textural layering.
Bladed	bld	Elongate to tabular platy crystals.
Botryoidal	bot	Aggregate of spherical shapes (also termed globular).
Clastic	cl	Fragmental with or without evidence of reworking.
Chalcopyrite disease		Fine inclusions (emulsion) of chalcopyrite in sphalerite.
Cockade	cock	Open-space vein filling in successive comb-like crusts.
Colloform	col	Finely laminated texture formed by rhythmic precipitation.
Dendritic	den	Minerals deposited in a fine branching pattern.
Disseminated	dis	Discrete grains or aggregates of a mineral distributed throughout a rock.
Druse	dr	A mineral surface covered with small projecting crystals.
Felted	fel	Lath-shaped crystals interwoven in an irregular fashion.
Framboidal	frm	Spheroidal aggregates of microscopic grains.
Granular	gran	Aggregates of crystals with a sugary texture.
Intergrown	ig	Minerals with shared grain boundaries and textures.
Interstitial	int	Occupying the space between other mineral phases.
Massive	msv	Uniform, essentially monomineralic material.
Matrix	mat	Minerals occurring as fine material between clasts in fragmental rocks.
Nodular	nod	Discrete subrounded aggregates, commonly colloform or radial mineral growths.
Poikilitic	poi	Mineral grains included as fine inclusions within the crystal of another mineral.
Porous	por	Texture with >10% open pore spaces.
Pseudomorph	pse	Replacement of one mineral by another with retention of the original crystal form.
Radial	rad	Mineral aggregates formed by growth radiating from a single point.
Relict	rel	Remnants of sulfide grains that have been partially dissolved or replaced.
Skeletal	skel	Development of the outline of a crystal without complete infill.
Sooty	soot	Extremely fine grained mineral that is not visible optically but is sufficiently abundant to color its matrix.
Veined	vnd	Mineral crosscut by veins of another material.
Vermicular	vrn	Wormlike intergrowths of one mineral with another.
Vuggy	vug	Rock containing coarse (<2 mm) pore spaces.
Additional textural terms applied to veins:		
Anastomosing	ana	Mutually intersecting vein network.
Barren	bar	No sulfide minerals in vein fill.
Branching	bra	Single vein split into two or more veins.
Halo	hal	Alteration extending outside the vein into wallrock (note difference with selvage).
Parallel	par	Two or more veins with the same orientation.
Selvage	sel	Mineral precipitation along edge of vein at contact with wallrock (note difference with halo).

**Table T6.** Grain-size classification for minerals.

Classification	Abbreviation	Size (mm)
Extremely fine grained	efg	<0.001
Very fine grained	vfg	0.001-0.5
Fine grained	fg	>0.5-1
Medium grained	mg	>1-2
Coarse grained	cg	>2

**Table T7.** Classification of sulfide samples and other hydrothermal precipitates recovered during Leg 193.

Type and textural description	Sulfide minerals	Gangue minerals	Major features/comments
1. Disseminated sulfide: widely dispersed disseminations of pyrite in altered volcanic rock.	Trace to minor fine to fine-grained pyrite, typically subhedral to euhedral. Extremely fine grained pyrite, confirmed by X-ray diffraction, turns its host anhydrite-silica-clay black. Fine-grained black (Fe rich) sphalerite and chalcopyrite in some samples.	Major to minor anhydrite, silica, and clay minerals.	Part of the intense pervasive alteration. Commonly also contains a fine network of thin (<0.5 mm) veinlets. Sphalerite is paragenetically later than pyrite.
2. Anhydrite ± quartz-pyrite vein: coarse to fine clear anhydrite crystals with or without quartz (or undifferentiated silica) and clay.	Trace to minor euhedral fine-grained pyrite.	Major coarse tabular anhydrite. Minor to major granular or euhedral quartz. Trace to minor fine-grained octahedral magnetite.	Fluid inclusions in the anhydrite. Pyrite forms a druse on the anhydrite. Paragenesis is anhydrite or quartz followed by pyrite.
2a. Vesicle linings of anhydrite quartz-pyrite: some have been accessed by an anhydrite ± quartz-pyrite veinlet.			Walls of some vesicles are silicified. Amount of sulfide depends on number of vesicles. Most, but not all, samples have <5% sulfide.
3. Anhydrite-magnetite ± pyrite veins: magnetite and pyrite as disseminations and in anhydrite veinlets with distinct alteration halos cutting a matrix of anhydrite, silica, and clay minerals. Some aggregates of magnetite have a spherical shape.	Trace to minor very fine grained magnetite and pyrite. Interstitial chalcopyrite and trace yellow sphalerite.	Major to minor very fine grained anhydrite, quartz, and clay.	Magnetite is in small vugs in anhydrite. Magnetite can have a spherical to framboidal shape.

Note: By convention, samples contain ≥ 5% sulfide.



**Table T9.** Structural geology checklist for descriptions.

---

Veins/fractures:

- Orientation
- Average width
- Mineral infilling
- Fabric
- Crack seal events
- Wall rock alteration
- Crosscutting relations of veins

Shear zones:

- Thickness
- Lineations
- Shear sense
- Deformation bands
  - Color
  - Thickness
  - Mineral composition
  - Number of bands within array

Breccias:

- Matrix or clast supported
- Matrix composition
- Clast size
- Angularity of clasts
- Clast composition

Igneous structures:

- Flow banding
  - Orientation of phenocrysts
  - Orientation of vesicles
-

**Table T10.** Aerobic and anaerobic cultivation media.

Media components	Aerobic	Anaerobic
Peptone	3 g	3 g
Yeast extract	1 g	1 g
Glucose	3 g	3 g
Elemental sulfur	50 mL	50 mL
Trace elements components	10 mL	10 mL
Resazurin solution (0.2 g/L)	—	5 mL
Cysteine-HCl	—	10 mL
Artificial seawater	1 L	1 L

Notes: Elemental sulfur was sterilized by steaming for 1 hr at 100°C on three successive days. Trace element components (1 L); CuSO<sub>4</sub> (0.01 g), ZnSO<sub>4</sub> (0.1 g), CoCl<sub>2</sub> (0.005 g), MnCl<sub>2</sub> (0.2 g), Na<sub>2</sub>MoO<sub>4</sub> (0.1 g), KI (0.05 g), LiCl (0.05 g), H<sub>2</sub>WO<sub>4</sub> (0.005 g) NaSO<sub>4</sub> (0.005 g), BaCl<sub>2</sub> (0.005 g).

**Table T11.** Tool strings, special tools, and log acronyms, Leg 193.

Tool string	Tool	Output	Physical significance	Units	
Triple-combination	HNCS*		Hostile environment natural gamma-ray sonde		
		HSGR	Standard (total) gamma ray	gAPI	
		HCGR	Computed gamma ray (HSGR—uranium contribution)	gAPI	
		HFK	Potassium	wt%	
		HTHO	Thorium	ppm	
		HURA	Uranium	ppm	
	APS*		Accelerator porosity sonde		
		APLC	Near array porosity	%	
		FPLC	Far array porosity	%	
		SIGF	Neutron capture cross section of the formation ( $\Sigma_f$ )	cu	
		STOF	Tool standoff (computed distance from borehole wall)	in	
	HLDS*		Hostile environment lithodensity sonde		
		RHOM	Bulk density	g/cm <sup>3</sup>	
		PEFL	Photoelectric effect	barn/e <sup>-</sup>	
		LCAL	Caliper—measure of borehole diameter	in	
		DRH	Bulk density correction	g/cm <sup>3</sup>	
	DIT		Phasor dual induction		
	SFR*		Spherically focused resistivity tool		
		IDPH	Deep induction phasor—processed resistivity	$\Omega$ m	
		IMPH	Medium induction phasor—processed resistivity, medium	$\Omega$ m	
SFLU		Shallow spherically focused resistivity	$\Omega$ m		
FMS*-sonic	NGT*		Natural gamma-ray tool		
		SGR	Standard (total) gamma ray	gAPI	
		CGR	Computed gamma ray (SGR – uranium contribution)	gAPI	
		POTA	Potassium	Wet wt%	
		THOR	Thorium	ppm	
		URAN	Uranium	ppm	
	DSI*		Dipole shear sonic imager		
		DTCO	Compressional wave transit time	$\mu$ s/ft	
		DTSM	Shear wave transit time	$\mu$ s/ft	
		DTST	Stoneley wave transit time	$\mu$ s/ft	
	GPIT*		General purpose inclinometer tool		
		Fx, Fy, Fz	Magnetic field (three orthogonal directions)	oer	
	FMS*		Formation microscanner		
			Oriented images of borehole wall microresistivity	$\Omega$ m	
	UHT-MSM	UHT-MSM		Ultra high temperature multisensor memory tool	
			T <sub>extr</sub> T <sub>int</sub>	Temperature (external borehole and internal tool) Pressure	$^{\circ}$ C psi
	HTT	HTT		LDEO high-temperature tool Temperature	$^{\circ}$ C
LWD	RAB*		Resistivity at the bit		
		BD, BM, BS	Oriented images	$\Omega$ m	
		R <sub>RING</sub>	Ring resistivity	$\Omega$ m	
		R <sub>BIT</sub>	Bit resistivity	$\Omega$ m	
		Res_BD	Resistivity deep	$\Omega$ m	
		Res_BM	Resistivity medium	$\Omega$ m	
		Res_BS	Resistivity shallow	$\Omega$ m	
GR_RAB	Gamma ray	gAPI			

Note: \* = Trademark of Schlumberger.

**Table T12.** Wireline tool strings and properties measured, Leg 193.

Tool string	Logging speed (m/hr)	Individual tools	Properties measured	Tool length (m)	Sample interval (cm)	Vertical resolution (cm)	Maximum temperature (°C)
Triple combination	488	HNGS*	Natural gamma ray	2.59	15	45	260
		APS*	Porosity	3.96	5 and 15	30	175
		HLDS*	Bulk density, photoelectric factor	7.03	15	38	175
		DIT-SFR*	Resistivity	9.53	15	200/150/76	175
FMS* sonic	250	FMS*	Resistivity image	7.72	0.25	0.5	175
		NGT*	Natural gamma ray	2.61	15	45	150
		GPIT*	Tool orientation, magnetic field	(in FMS)	1 or 15	NA	175
		DSI*	Sonic velocity	15.5	15	110	175
UHT-MSM	200	UHT-MSM	Temperature	NA	NA	NA	232 (~10 hr) 400 (~4 hr)
HTT	200	HTT	Temperature	NA	NA	NA	275
LWD		RAB*	Resistivity image	10.1 ft	1/20 s	NA	150
			Electrical resistivity	NA	(~15 cm)	NA	NA
			Gamma ray	NA	NA	NA	NA

Notes: \* = trademark of Schlumberger. See Table T11, p. 71, for explanations of acronyms used to describe tool strings and individual tool names. NA = not applicable.